Brazilian Journal
of Chemical
Engineering

ISSN 0104-6632
Printed in Brazil
www.abeq.org.br/bjche

Vol. 34, No. 02, pp. 507 - 530, April - June, 2017
dx.doi.org/10.1590/0104-6632.20170342s20150504

TWO-DIMENSIONAL FLOW OF POWER-LAW FLUIDS OVER A PAIR OF CYLINDERS IN A SIDE-BY-SIDE ARRANGEMENT IN THE LAMINAR REGIME

Saroj K. Panda*

Department of Chemical Engineering, Indian Institute of Technology Delhi
New Delhi 110016, India
Tel.: +91 11 2659 6282, fax: +91 11 2658 1120
Email: sarojdeep@gmail.com

(Submitted: August 23, 2015; Revised: February 20, 2016; Accepted: March 29, 2016)

Abstract – This manuscript presents the effect of Reynolds number (*Re*) and proximity of the bodies on the hydrodynamics of flow of shear-thinning, Newtonian and shear-thickening fluids over a pair of cylinders kept in side-by-side arrangement. Results obtained from the numerical simulations carried out with a combination of different parameters in the range of $0.2 \leq$ power law index (n) ≤ 1.8, $0.1 \leq Re \leq 100$ and $1.2 \leq G$ (gap between the cylinders/diameter) ≤ 4 have been discussed in details. Analysis of the results gives a clear insight into the complex influence of *Re* on streamline patterns, surface pressure profiles, drag and lift coefficients for various fluids when the gap between two cylinder is changed.

Keywords: Reynolds number; power-law fluids; gap ratio; pressure coefficient; drag-lift.

INTRODUCTION

In day to day life, many systems are encountered where fluid flow occurs over cylindrical bodies. These ordinary looking systems practically exhibit a rich variety of flow phenomena. Different flow regimes are encountered depending on the velocity of the fluid, size of the cylinders and the proximity of the cylinders to the neighboring bodies. Needless to say the fundamental change at the microscopic level is manifested at the macroscopic level, resulting in different scaling in the drag and lift forces and coefficients of heat and mass transfer etc. Therefore, the study of flow over a circular cylinder has drawn considerable attention over the last few decades. Consequently, over the years, a voluminous body of information on the hydrodynamics of the flow of Newtonian fluids over a circular cylinder has been accrued. The available information is excellently summarized in two books by Zdravkovich (Zdravkovich, 1997, 2003). Though the studies on flow over a solitary cylinder gives us valuable insights into the flow phenomena, these do not depict the reality for the cases where flow occurs over multiple cylinders as the hydrodynamics is dependent on the proximity and arrangement of the cylinders. As an example, in a shell and tube heat exchanger the area for heat transfer increases with the increase in number of tubes, but at the same time this may lead to a large pressure drop unless the size and the shape of the flow path are properly chosen. Likewise, there are several systems such as aerosol filters based on hollow fiber modules, polymer and paper coating applications, food processing industry and recycling plants where the arrangement of cylinders affects the flow pattern. Despite such pragmatic significance, there

*To whom correspondence should be addressed

have been very few studies involving multiple cylinders.

It is also readily acknowledged that most high molecular weight and multiphase systems encountered in a broad spectrum of chemical, polymer, food, agro-chemicals, biotechnological and process engineering applications display shear-thinning behavior (Bird et al., 1987; Steffe, 1996; Chhabra and Richardson, 1999). This type of non-Newtonian flow behavior is conveniently approximated by the power-law model (Bird et al., 1987; Steffe, 1996; Chhabra and Richardson, 1999). Despite the wide occurrence of shear-thinning behavior in scores of industrial settings, very little is known about the flow around a group of cylinders, albeit a reasonable body of knowledge has evolved over the past 10-15 years as far as a single cylinder is concerned. Therefore, the present work is concerned with the flow over a two-cylinder assembly in a side-by-side arrangement. In particular, consideration is given to the role of non-Newtonian flow characteristics and of the spacing between the two cylinders on the detailed kinematics of the flow, as well as on the drag and lift coefficients of each cylinder. It is, however, instructive and useful to briefly recount the flow of power-law fluids past a cylinder and that of Newtonian fluids over a side-by-side arrangement of cylinders to facilitate the presentation and discussion of the new results reported herein.

PREVIOUS WORK

As noted earlier, a wide range of literature is available on various aspects of the flow over a single cylinder submerged in Newtonian fluids (Morgan, 1975; Zdravkovich, 1997, 2003), though there are still unresolved issues, especially at high Reynolds numbers. On the other hand, the analogous literature on the flow of power-law fluids past a cylinder is not only of recent vintage but is also much less extensive. Some numerical results are now available on hydrodynamics (D'Allessio and Pascal, 1996; Whitney and Rodin, 2001; Chhabra et al., 2004; Bharti et al., 2006, 2007), forced convection heat transfer (Soares et al., 2005; Bharti et al., 2007), and mixed convection heat transfer (Srinivas et al., 2009; Soares et al., 2009; Bouaziz et al., 2010). However, most of these studies are restricted to the steady flow regime (Sivakumar et al., 2006), very few studies deal with the flow of power-law fluids past a cylinder (Patnana et al., 2009), and heat transfer (Patnana et al., 2010; Soares et al., 2010), in the laminar vortex shedding regime. These studies (Patnana et al., 2009, 2010; Soares et al., 2010), signify that all else being equal, shear-thinning behavior enhances the hydrodynamic drag. The effect on drag is particularly striking at low Reynolds number. Besides the aforementioned studies based on the numerical solution of the complete governing equations, some works have been carried out employing standard boundary layer flow approximations to obtain approximate expressions for skin friction and Nusselt number (Khan et al., 2006). A few experimental studies on flow of non-Newtonian fluids past a cylinder have also been reported (Coelho and Pinho, 2003), which elucidate the roles of visco-elastic and shear-thinning behavior on the vortex shedding characteristics. Since the fluids used in most of the studies display both elastic and shear-thinning characteristics, it is difficult to delineate their individual contributions unless the special flow classification criteria are used (Astarita, 1979; Thompson and Mendes, 2005). Therefore, possibilities of detailed comparison between the prediction and experimental observation are excluded.

The flow over two-cylinders of equal size arranged in different configurations represents the simplest possible model to study the hydrodynamics of the flow over a group of cylinders. In this case, the flow is influenced not only by the value of Reynolds number (Williamson, 1985; Meneghini et al., 2001; Chitanya and Dhiman, 2012), but also by the center-to-center distance between the two cylinders (Bearman and Wadcock, 1973; Williamson, 1985; Chitanya and Dhiman, 2012). The flow characteristic also changes depending on the geometrical configuration of cylinders such as side-by-side (Bearman and Wadcock, 1973; Kang, 2003; Chitanya and Dhiman, 2012) and tandem (Meneghini et al., 2001; Juncu, 2007(2); Patil et al., 2008).

A cursory inspection of the available literature (Zdravkovich, 1977, 1987, 1997, 2003; Kang, 2003; Juncu, 2007; Liang et al., 2009; Ryu et al., 2009; Tsutsui, 2010; Shyam et al., 2013) reveals that the bulk of the information relates to high Reynolds numbers like those encountered in air/gas, air/liquid heat exchangers. On the other hand, owing to the generally high viscosity levels of the multiphase (foams, suspensions, and emulsions) and polymeric systems, the representative Reynolds numbers in polymer, food and slurry related applications seldom exceed 20-30. Few studies have been reported on flow over multiple cylinders (Zhang et al., 2001; Huang et al., 2006), which take Reynolds numbers in different flow regimes into account. Especially, the studies on non-Newtonian fluids that provide detailed information on the pressure distribution in the flow field, variation of drag and lift forces over a wide range of Reynolds number are rare. Knowledge of the pressure distribution in a flow field in the presence of multiple cylinders is not only important to optimize the design efficiently but also of interest to ensure the safety and longevity of the critical components in some of the applications. In addition, to ensure the stability of the components, the study of drag characteristics of flow of both the Newtonian and power-law fluids in both high as well as low Reynolds number regimes is also of industrial interest. Considering the practical importance of the information on flow over multiple cylinders using Newtonian and power-law fluids, the present work is carried out. In this work, the flow patterns of both Newtonian and power-law fluids when passed over two cylinders kept in

side-by-side arrangement are studied numerically, over a wide range of Reynolds number from 0.1-100. In addition to the effect of Reynolds number, the effects of power-law index and the gap between the two cylinders on pressure coefficients, drag and lift coefficients are analyzed in detail. The behavior of shear-thinning fluid has also been compared with that of the Newtonian and shear-thickening fluids under a few selected conditions.

PROBLEM STATEMENT AND GOVERNING EQUATIONS

Physical arrangement of the cylinders and the flow are schematically illustrated in Figure 1 (a). The circular cylinders shown in this figure are infinitely long in the z-direction and are of equal radius *R* and diameter *D*. The flow considered here is two-dimensional, incompressible, with uniform inlet velocity U_o. Based on the available literature (Kang, 2003; Sivakumar et al., 2006), flow for both Newtonian and power-law fluids is initially assumed to be steady up to *Re* = 40 and unsteady for *Re* > 40. To ascertain that the flow is indeed steady up to *Re* = 40, over the range of conditions used here, a few preliminary time-dependent simulations for extreme values of parameters (*Re*, *G*, *n*) are performed. Also unsteady calculations are carried out for high Reynolds number (*Re* = 100) to see the effect of all parameters (*Re*, *G*, *n*) in the power-law regime. Since it is not possible to simulate an unconfined flow numerically, it is customary to introduce an artificial domain in the form of a box as shown in Figure 1 (b). In the figure, the cylinders are placed inside a square of size *H*, with a gap of *G* in such a way that the mid-point between the two cylinders coincides with the center of the box. The value of *H* is chosen in such a manner that the study is carried out with modest computational resources without influencing the flow field. The results obtained from the time dependent study indicate that the flow is steady in the range *Re* = 0.1 - 40 and is in agreement with the available literature (Kang, 2003; Sivakumar et al., 2006). The flow becomes unsteady in the range *Re* = 40 - 100. To characterize the flow of both Newtonian and power-law fluid, in both steady and unsteady domain, the continuity and momentum equations are solved. The governing equations in their dimensionless form are given below.

Continuity equations in cartesian form:

$$\frac{\partial U_x}{\partial x}+\frac{\partial U_y}{\partial y}=0 \tag{1}$$

Momentum equations in cartesian form for the *x*- and *y*- directions:

x-momentum equation (2)

$$\frac{\partial U_x}{\partial t}+\frac{\partial\left(U_xU_x\right)}{\partial x}+\frac{\partial\left(U_xU_y\right)}{\partial y}=-\frac{\partial P}{\partial x}+\frac{1}{\mathrm{Re}}\left(\frac{\partial \tau_{xx}}{\partial x}+\frac{\partial \tau_{yx}}{\partial y}\right)$$

y-momentum equation (3)

$$\frac{\partial U_y}{\partial t}+\frac{\partial\left(U_xU_y\right)}{\partial x}+\frac{\partial\left(U_yU_y\right)}{\partial y}=-\frac{\partial P}{\partial y}+\frac{1}{\mathrm{Re}}\left(\frac{\partial \tau_{xy}}{\partial x}+\frac{\partial \tau_{yy}}{\partial y}\right)$$

For power-law fluids, the extra stress tensor τ_{ij} is related to the rate of deformation tensor (ε_{ij}) and is expressed as:

$$\tau_{ij}=2\eta\varepsilon_{ij} \tag{4}$$

where the rate of deformation tensor is given by:

$$\varepsilon_{ij}=\frac{1}{2}\left(\frac{\partial U_i}{\partial x_j}+\frac{\partial U_j}{\partial x_i}\right) \tag{5}$$

and the viscosity, η, for a power-law fluid is given by

$$\eta=m\left(2I_2\right)^{\frac{n-1}{2}} \tag{6}$$

where *n* is the power-law index. While *n* =1 corresponds to the Newtonian behavior, *n* < 1 denotes the shear-thinning behavior of fluid. I_2 is the second invariant of the rate of deformation tensor and expressed as (Bird et al., 2002):

$$I_2=\sum_i\sum_j\varepsilon_{ij}.\varepsilon_{ji}=\varepsilon_{xx}^2+\varepsilon_{xy}^2+\varepsilon_{yx}^2+\varepsilon_{yy}^2 \tag{7}$$

The physically realistic boundary conditions for this flow are written as follows:

(i) At the inlet plane: The uniform flow in x-direction is prescribed, i.e.,

$$U_x=U_0\ ;\ U_y=0 \tag{8}$$

(ii) The *top and bottom walls* are assumed to be slip boundaries so that there is no dissipation at these walls. In mathematical terms, these are expressed as:

$$\frac{\partial U_x}{\partial y}=0\quad ;\quad U_y=0 \tag{9}$$

(iii) On the surface of the solid cylinders: The standard no-slip boundary condition is used, i.e.,

$$U_x=0\ ;\ U_y=0 \tag{10}$$

(iv) At the exit plane: The default outflow boundary condition option in *FLUENT* (a zero diffusion flux for all flow variables) was used in this work. This choice implies that the conditions of the outflow plane are extrapolated from within the domain and this extrapolation procedure has negligible influence on

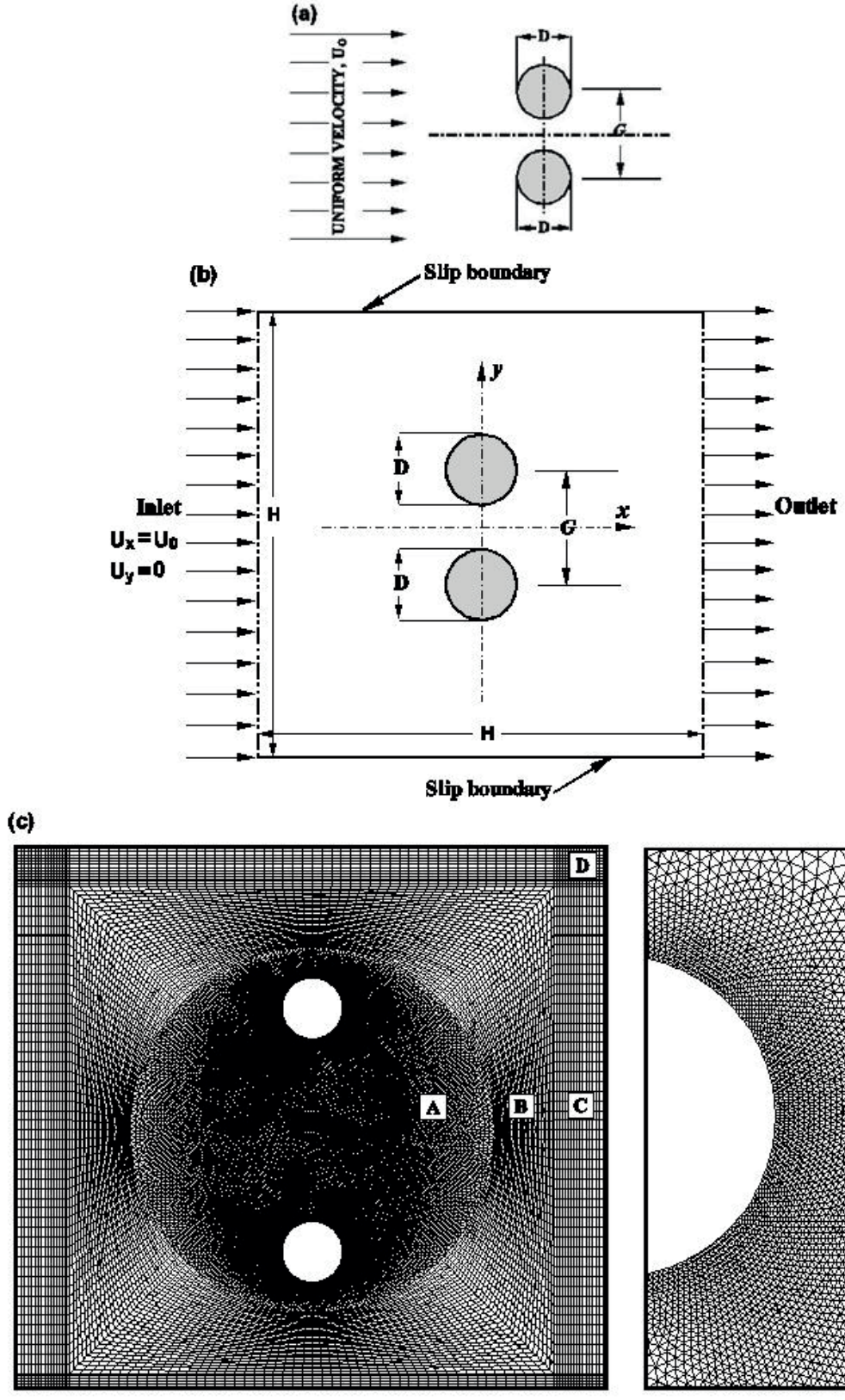

Figure 1. (a) Schematic representation of the physical model (b) Computational domain (c) Close up view of the grid in the vicinity of cylinders.

the upstream flow conditions. Furthermore, the scheme used by *FLUENT* updates the outflow velocity and pressure in a manner that is consistent with the fully developed flow assumption, when there is no area change at the outflow boundary. However, the gradients in the cross-stream direction may still exist at the outflow boundary. This is similar to the homogeneous Neumann condition, that is,

$$\frac{\partial U_x}{\partial x} = 0 \; ; \; \frac{\partial U_y}{\partial x} = 0 \tag{11}$$

The numerical solution of the governing equations (1), (2) and (3), together with the aforementioned boundary conditions, maps the flow domain in terms of the primitive variables, namely, U_x, U_y and P. These variables are post-processed to evaluate the derived quantities such as stream function, surface pressure coefficients, drag and lift coefficients as functions of the pertinent governing parameters. At this juncture, it is appropriate to introduce the definitions of some of these, as well as the other relevant parameters.

In this work, the free stream velocity, U_0, and diameter of the cylinder, D, are used as scaling variables. Thus, the pressure is scaled using ρU_0^2 , stress components using $m\left(\frac{U_0}{D}\right)^n$, time with $\frac{D}{U_0}$. Furthermore, the flow is governed by three dimensionless groups, namely, the Reynolds number (*Re)*, power-law index (*n)*, and the non-dimensional gap spacing (*G*).

Reynolds number (*Re*) is expressed as

$$Re = \frac{\rho U_0^{2-n} D^n}{m} \tag{12}$$

and the non-dimensional gap spacing is expressed as

$$G = \frac{g}{D} \tag{13}$$

Total drag (C_D), pressure drag (C_{DP}) and friction drag (C_{DF}) coefficients are written as

$$C_D = \frac{2F_D}{\rho U_0^{\,2} D}, \quad C_{DP} = \frac{2F_{DP}}{\rho U_0^2 D} = \int_S C_P n_x dS \quad \text{and}$$
$$C_{DF} = \frac{2F_{DF}}{\rho U_0^2 D} = \frac{2^{n+1}}{\mathrm{Re}} \int_S \left(\tau \cdot n_s\right) dS \tag{14}$$

where C_D is the drag force in the direction of flow exerted on the cylinder per unit length. It is also customary to split the total drag force into two components arising from the shear and pressure forces. The parameters that represent the shear force and pressure components are referred to as the friction drag coefficient (C_{DF}) and pressure drag coefficient (C_{DP}), respectively.

The non-dimensional parameter that is used to represent the lift is referred to as the lift coefficient (C_L) and given as:

$$C_L = \frac{2F_L}{\rho U_0^{\,2} D} \tag{15}$$

where F_L is the lift force acting in the y-direction on the cylinder per unit length. The lift force also has two components, i.e., shear and pressure. These components are represented by two dimensionless parameters known as the pressure lift coefficient (C_{LP}) and friction lift coefficient (C_{LF}).

To get the information about the pressure distribution on the surface of the cylinders, the surface pressure coefficient (C_P) is calculated and expressed as:

$$C_P = \frac{\text{Static pressure}}{\text{Dynamic pressure}} = \frac{p - P_\infty}{\frac{1}{2}\rho_\infty U_0^{\,2}} \tag{16}$$

where p is the local pressure at a point on the surface of the cylinder and P_∞ is its reference value far away from the cylinder.

In this work, the vortex shedding frequency (f) is calculated for the unsteady flow regime (Re = 100) from the time history of the lift coefficient (C_L). The time period (T) has been calculated based on 10 constant periodic cycles.

NUMERICAL SOLUTION METHOD

In this study, the field equations are solved using *FLUENT,* whereas a third-party software is used for creating a suitable solution mesh. Different regions of the grid structure used for the present study are shown in Figure 1(c). Fine unstructured triangular cells are generated in the region close to the cylinder (region A) where the gradients are expected to be steep. In all other regions (B, C and D), quadrilateral cells are used and the grid is stretched from fine to coarse using the 'successive ratio' stretching function.

The two-dimensional, laminar, segregated solver is used to solve the incompressible flow on the collocated grid arrangement. Both steady and unsteady solvers are used in this study. The detailed description of the numerical solution procedure is available in our earlier papers (Panda and Chhabra, 2010, 2011). To ascertain the prediction of the solver at high Reynolds number, flow patterns of both Newtonian and power-law fluids are obtained and can be validated using the results reported by Kang (2003). For discretizing the convective terms in the momentum equations a second order upwind scheme is used, whereas semi-implicit method for the pressure linked equations

(*SIMPLE*) scheme is used for solving the pressure-velocity coupling. A time-integration second order implicit scheme is used with time step size (Δt) of 0.01. A through time dependent study is carried out to arrive at an optimum value of Δt. The physical properties of the flow are given as input using *constant density* and *non-Newtonian power-law viscosity* modules. Minimum and maximum viscosities of the fluid used in the simulations are 0 and 1e20 Kg/m-s, respectively. The physical properties such as ρ, *m*, *n* used for this work are given in Table 1. The input values of these physical properties and kinematic parameters such as *D*, U_0, **Ω**, etc. are of no consequence as the final results are reported in a dimensionless form. It must be noted here that the present simulations do not consider the effect of gravitational force on the flow. *FLUENT* solves the system of algebraic equations using the Gauss-Siedel (G-S) point-by-point iterative method in conjunction with the algebraic multi-grid (AMG) method solver. The use of the AMG scheme greatly reduces the number of iterations (thereby accelerating convergence) and thus economizing the CPU time required to obtain a converged solution, particularly when the model contains a large number of control volumes. For the present study, a relative convergence criterion of 10^{-8} is used for the residuals of the continuity and *x*- and *y*- components of the momentum equations. A simulation is deemed to have converged when the values of the global parameters stabilize to at least four significant digits.

Table 1. Physical properties of the fluid used

Re	ρ (Kg/m³)	m (Kg/m-s)					
		n = 0.2	n = 0.4	n = 0.6	n = 0.8	n = 1	n = 1.2
0.1	0.1	0.01584	0.02511	0.03981	0.06309	0.1	0.15848
0.2	0.2	0.01584	0.02511	0.03981	0.06309	0.1	0.15848
0.5	0.5	0.01584	0.02511	0.03981	0.06309	0.1	0.15848
1	1	0.01584	0.02511	0.03981	0.06309	0.1	0.15848
2	2	0.01584	0.02511	0.03981	0.06309	0.1	0.15848
5	5	0.01584	0.02511	0.03981	0.06309	0.1	0.15848
10	10	0.01584	0.02511	0.03981	0.06309	0.1	0.15848
20	20	0.01584	0.02511	0.03981	0.06309	0.1	0.15848
30	30	0.01584	0.02511	0.03981	0.06309	0.1	0.15848
40	40	0.01584	0.02511	0.03981	0.06309	0.1	0.15848
100	100	0.01584	0.02511	0.03981	0.06309	0.1	0.15848

Table 2. Selection of optimum domain at *Re* = 0.1

H/D	***Re = 0.1, n = 1, G = 4***							
	Upper Cylinder				**Lower Cylinder**			
	C_{DP}	C_D	C_{LP}	C_L	C_{DP}	C_D	C_{LP}	C_L
220	21.6440	43.7499	1.9171	3.8090	21.6429	43.7506	-1.9194	-3.8081
240	21.3989	43.2549	1.8931	3.7618	21.3979	43.2556	-1.8954	-3.7610
260	21.3984	43.2546	1.8924	3.7612	21.3981	43.2558	-1.8955	-3.7625
H/D	***Re = 0.1, n = 0.2, G = 4***							
	Upper Cylinder				**Lower Cylinder**			
	C_{DP}	C_D	C_{LP}	C_L	C_{DP}	C_D	C_{LP}	C_L
220	183.551	262.335	0.6632	-0.8828	183.541	262.325	0.6312	0.8464
240	183.581	262.378	-0.6704	-0.8927	183.571	262.369	0.6375	0.8553
260	183.542	262.338	-0.6724	-0.8962	183.568	262.364	0.6324	0.8592

Table 3. Selection of optimum domain at *Re* = 5

H/D	***Re = 5, n = 1, G = 4***							
	Upper Cylinder				**Lower Cylinder**			
	C_{DP}	C_D	C_{LP}	C_L	C_{DP}	C_D	C_{LP}	C_L
100	2.2058	4.2072	0.3475	0.6494	2.2058	4.2072	-0.3477	-0.6491
120	2.1853	4.1696	0.3464	0.6475	2.1853	4.1697	-0.3466	-0.6472
180	2.1838	4.1706	0.3458	0.6470	2.1855	4.1710	-0.3465	-0.6485
H/D	***Re = 5, n = 0.2, G = 4***							
	Upper Cylinder				**Lower Cylinder**			
	C_{DP}	C_D	C_{LP}	C_L	C_{DP}	C_D	C_{LP}	C_L
100	4.2432	5.8273	-0.021	-0.032	4.2433	5.8275	0.0201	0.0308
120	4.2447	5.8290	-0.021	-0.032	4.2448	5.8293	0.0200	0.0308
180	4.2454	5.8297	-0.021	-0.032	4.2454	5.8299	0.0201	0.0309

CHOICE OF NUMERICAL PARAMETERS

It is well known that the reliability and accuracy of the numerical results are dependent on a prudent choice of the numerical parameters, namely, the optimal domain size (H), grid characteristics (number of cells on the surface of the cylinder, grid spacing, stretching, etc.) and to some extent by the convergence criterion, etc. (Roache, 1994; Sivakumar et al., 2007; Patil et al., 2008; Sahu et al., 2009). In this work, the values of these parameters have been selected after extensive exploration by varying their values within $100 \leq H / D \leq 300$. Due to the slow spatial decay of the velocity field at low Reynolds numbers, the required domain size decreases with increasing Reynolds number. For this purpose, the values of Re = 0.1 and 5 are taken to be representative of the *low* and *high* Reynolds number region. The results summarized in Tables 2 and 3 show the influence of (H/D) on C_D, C_{DP}, C_L and C_{LP} for two different values of Reynolds number (Re = 0.1 and 5), two extreme values of power-law index (n = 1 and 0.2) and for G = 4. From the analysis of these results obtained from the domain independent study, (H / D) = 240 is chosen for Re < 5 whereas (H / D) = 120 is selected for Re ≥ 5 studies to nullify the domain effect. It must be noted here that the domain used in this study is much larger than that used by others (Kang, 2003).

Table 4. Details of grids used for the grid independence study

Grid	H/D = 240			
	N_i	N	M	N_{cells}
G1	100	5	16	48550
G2	200	10	33	196254
G3	400	20	66	782224

Grid	H/D = 120			
	N_i	N	M	N_{cells}
G1	100	5	16	37780
G2	200	10	33	153054
G3	400	20	66	609424

Ni = Number of points on the surface of the cylinder
N = Number of points in the 1st sub domain
M = Number of points in the 2nd sub domain

Similarly, an optimal grid is used to resolve the thin boundary layers and steep gradients near the cylinders without being prohibitively computationally intensive. To arrive at the choice of an optimal grid, the relative performances of the three grids were studied in details. Each grid was characterized in terms of the number of points (N_i) on the surface of cylinder and the value of (δ / D)near the cylinder, which are summarized in Table 4. A typical grid is shown in Figure 1(c). Tables 5 and 6 summarize the relative performance of each grid in terms of C_D, C_{DP}, C_L and C_{LP}. From the detailed analysis of these results, it is noted that very little is gained in terms of accuracy by moving from G2 to G3, however, the CPU time required for G3 is many fold higher than that needed for G2 to satisfy the same criterion of convergence. Therefore, grid G2 that denotes a good compromise between the accuracy and computational effort is chosen for the present study. Using the grid G2 and optimized domains, the two dimensional steady and unsteady flow computations were carried out. The parameters used for the present study are as follows:
Reynolds number, Re = 0.1, 0.2, 0.5, 1, 2, 5, 10, 20, 30, 40 and 100
Power-law index, n = 0.2, 0.4, 0.6, 0.8 and 1
Gap spacing, G = 1.2, 1.7, 2, 2.5 and 4

Table 5. Effect of grid details on the results at Re = 0.1 (H/D = 240)

Grid	***Re = 0.1, n = 1, G = 4***							
	Upper Cylinder				**Lower Cylinder**			
	C_{DP}	C_D	C_{LP}	C_L	C_{DP}	C_D	C_{LP}	C_L
G1	20.0215	42.2026	1.8351	3.3564	20.0225	42.2046	-1.8342	-3.3586
G2	21.3989	43.2549	1.8931	3.7618	21.3979	43.2556	-1.8954	-3.7610
G3	21.4007	43.2452	1.9020	3.7681	21.3906	43.2451	-1.8920	-3.7583
Grid	***Re = 0.1, n = 0.2, G = 4***							
	Upper Cylinder				**Lower Cylinder**			
	C_{DP}	C_D	C_{LP}	C_L	C_{DP}	C_D	C_{LP}	C_L
G1	179.338	255.226	-0.8358	-1.0313	179.312	255.182	0.8298	1.0223
G2	183.581	262.378	-0.6704	-0.8927	183.571	262.369	0.6375	0.8553
G3	183.301	261.990	-0.6722	-0.8955	183.423	262.112	0.6339	0.8504

Table 6. Effect of grid details on the results at Re = 5 (H/D = 120)

Grid	***Re = 5, n = 1, G = 4***							
	Upper Cylinder				**Lower Cylinder**			
	C_{DP}	C_D	C_{LP}	C_L	C_{DP}	C_D	C_{LP}	C_L
G1	2.1033	4.1561	0.3235	0.6356	2.1014	4.1512	-0.3227	-0.6438
G2	2.1853	4.1696	0.3464	0.6475	2.1853	4.1697	-0.3466	-0.6472
G3	2.1844	4.1633	0.3467	0.6488	2.1849	4.1658	-0.3459	-0.6483
Grid	***Re = 5, n = 0.2, G = 4***							
	Upper Cylinder				**Lower Cylinder**			
	C_{DP}	C_D	C_{LP}	C_L	C_{DP}	C_D	C_{LP}	C_L
G1	4.1291	5.8207	-0.035	-0.043	4.1321	5.8224	0.0355	0.0435
G2	4.2447	5.8290	-0.021	-0.032	4.2448	5.8293	0.0200	0.0308
G3	4.2431	5.8278	-0.020	-0.031	4.2444	5.8294	-0.0200	-0.0310

It is to be noted here that, for comparison of flow behavior of shear thinning fluid with that of the shear thickening fluid, some additional simulations have been carried out using power-law index 1.2, 1.6 and 1.8 at selected Reynolds numbers (0.1 and 40) at gap spacings of 1.2 and 4.

RESULTS AND DISCUSSION

Validation of Results

Prior to presenting new results of any numerical study, it is necessary to validate the numerical solution procedure to ascertain the accuracy and reliability of the results. Towards this end, some of the results obtained from this numerical analysis are presented in Table 6 along with the data reported by Kang (2003), Ding et al. (2007) and Chaitanya and Dhiman (2012) under similar conditions. Comparison of the data given in Table 7 signifies that the results obtained from the present study are in good agreement with the results reported by other researchers. The small deviations in values can be attributed to the different grid sizes, solution methodologies, size and shape of domain, convergence criterion, etc. (Roache, 1994) chosen for simulations.

Aside from the aforementioned comparisons, the credibility of the numerical solution methodology employed herein is verified by studying the flow of Newtonian and power-law fluids in the standard lid driven square cavity separately and thereafter comparing the results with available information (Ghia et al., 1982; Neofytou, 2005). The centerline velocities obtained from the present standard lid driven square cavity are found to be within ±2% of the corresponding Newtonian results (Ghia et al., 1982), and within ±2.5% for power-law fluids as reported by Neofytou (2005). Agreement of the results reported here with those reported by others demonstrates the credibility of the numerical solution methodology used for the present study. Based on the above mentioned comparison and past experience, the present results for the two cylinder configuration in power-law fluids are believed to be reliable to within ±1-2%.

Table 7. Comparison between the present and literature values for Re = 100 and 40; G = 2 and 4; n = 1

Upper Cylinder		
Source	C_D	C_L
Re = 40, n = 1, G = 2		
Present	1.7064	0.3665
Kang, 2003	1.70	0.3651
Re = 100, n = 1, G = 4		
Present	1.4686	--
Chaitanya and Dhiman, 2012	1.4727	--
Ding et al., 2007	1.514	--
Lower Cylinder		
Source	C_D	C_L
Re = 40, n = 1, G = 2		
Present	1.7066	-0.3658
Kang, 2003	1.70	-0.3706
Re = 100, n = 1, G = 4		
Present	1.4702	--
Chaitanya and Dhiman, 2012	1.4726	--
Ding et al., 2007	1.514	--

In Figure 2, only the vorticity contours for Re = 40 and 100 (for Newtonian fluids) for different gap ratios are presented to validate the flow patterns shown by Kang (2003) in their study. The patterns are (a) single bluff-body pattern (Re = 100, G = 1.2), (b) flip-flopping pattern (Re = 100, G = 1.7), (c) in-phase-synchronized pattern (Re = 100, G = 2.5), (d) anti-phase-synchronized pattern (Re = 100, G = 4) and (e) steady pattern (Re = 40, G = 2). The flow patterns presented here are in good agreement with those of Kang (2003). As observed, the wake patterns are highly dependent on the gap between the two cylinders. At G = 1.2, both cylinders act like a single body and vortices are formed periodically at both sides of the cylinders. The flow through the narrow gap between the cylinders has no real effect on the wake region, so complete suppression of narrow vortices occurs between the cylinders. This flow pattern is called 'single bluff-body pattern'. Upon increasing the gap from 1.2 to 1.7 (see Figure 2(b)), the flow encountered between the cylinders experiences a drag force from the cylinder surface and vortex shedding occurs in a highly irregular fashion. Such a flow structure is called 'flip-flopping pattern' as suggested by Kang (2003). When the gap is increased to 2.5, the vortices generated from the cylinders merge with each other at the initial stage, but separate far away from the cylinder in the downstream. This flow pattern is known as 'in-phase-synchronized pattern'. With a high gap ratio (at G = 4), the wakes formed are periodic in nature and formed separately from each cylinder. According to Kang (2003), the same drag coefficients are observed for both the cylinders and lift coefficients occur in anti-phase. So the pattern is referred to as an 'anti-phase-synchronized' pattern. At Re = 40 (G = 2), the flow is steady and symmetric about the mid-plane. No vortex shedding occurs in this case and the pattern is named as 'steady pattern'.

Detailed Flow Characteristics

The flow field is usually characterized by streamline profiles and surface pressure coefficients close to the cylinders as functions of the governing parameters. These functional relationships are presented in the following sections.

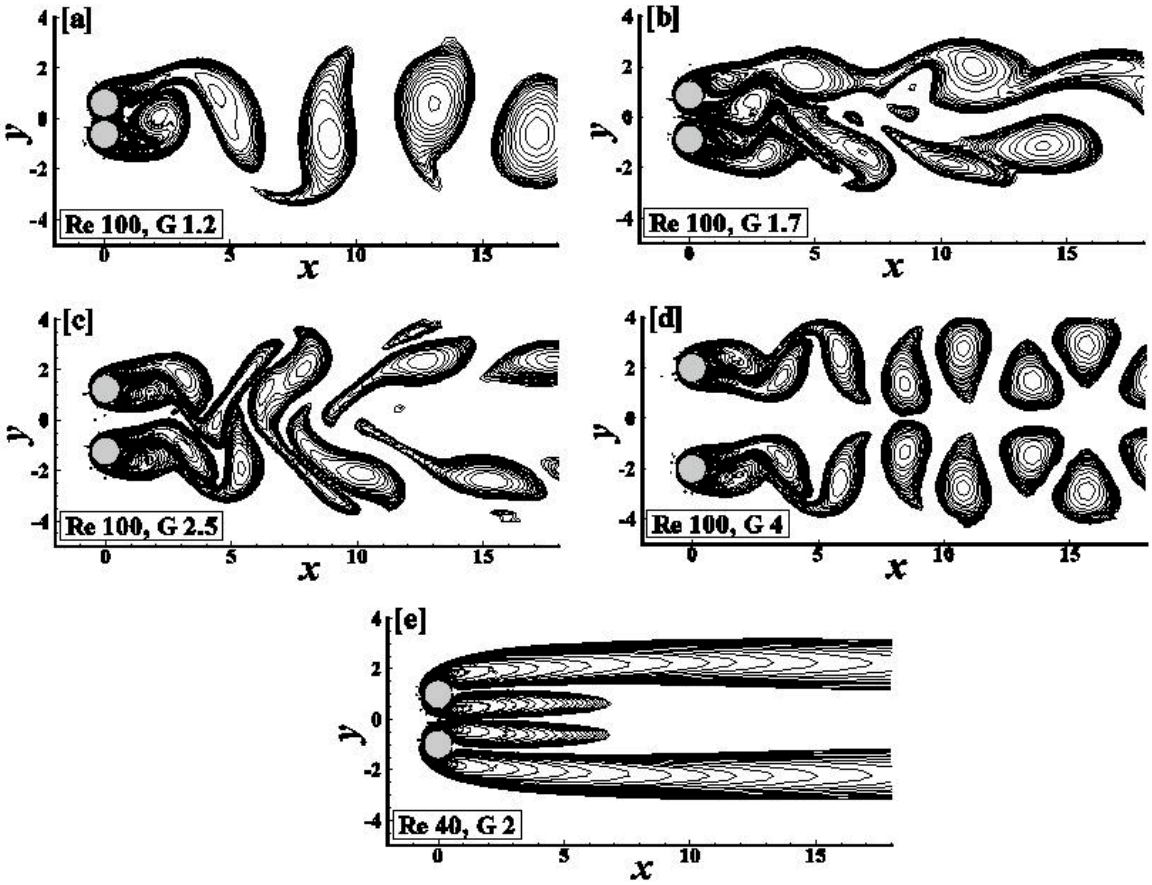

Figure 2. Vorticity contours for different wake patterns (a) single bluff-body pattern (Re=100, G=1.2); (b) flip-flopping pattern (Re=100, G=1.7); (c) in-phase-synchronized pattern (Re=100, G=2.5); (d) anti-phase- synchronized pattern (Re=100, G=4); (e) steady pattern (Re=40, G=2).

Streamline Profiles

Figure 3 shows the results elucidating the influence of *Re*, *G* and *n* on the streamlines in the vicinity of the cylinder. While Figure 3 (a) - (d) represent the streamlines obtained for Newtonian and shear-thinning fluids, Figure 3 (e) shows streamlines for shear-thickening fluid at selected conditions. For the range of Reynolds number used here, the flow is known to be steady ($0.1 \leq Re \leq 40$) and unsteady ($Re = 100$) for all values of the power-law index (n) and gap (G) between the two cylinders.

For shear-thinning fluids, the flow field is seen to be symmetric about the mid-plane at low *Re* (≤ 0.1) for all values of *G*. This is due to the fact that the viscous forces outweigh the inertial forces and a fluid element is able to follow the surface of the cylinders under these conditions. For fixed values of *n* and *G* with gradual increasing of *Re*, the flow field gets detached from the surface of the cylinder, which leads to the formation of the wake region in the rear end of the cylinder. This marks the formation of a pair of standing vortices at both cylinders, which grow independently with increasing value of *Re*, until *Re* attains a critical value.

For $G = 1.2$, $n = 0.2$, at very low *Re*, i.e., at 0.1 the streamlines show symmetry about the mid-plane and follow a very close path. When *Re* is increased beyond 10 no wake formation is observed. Finally, the flow field is detached from the cylinder surface at $Re = 40$ and 100, and a pair of vortices are formed at each cylinder.

At $G = 1.2$, with increasing power-law index from 0.2 to 1, no vortices are found at $Re = 0.1$. At this condition, even for shear-thickening fluid with $n = 1.2$ - 1.8 not much difference is observed in streamline profiles (Figure 3(e)). The streamline profile obtained for low gap ration and low value of *Re* resemble the streamline obtained for a single

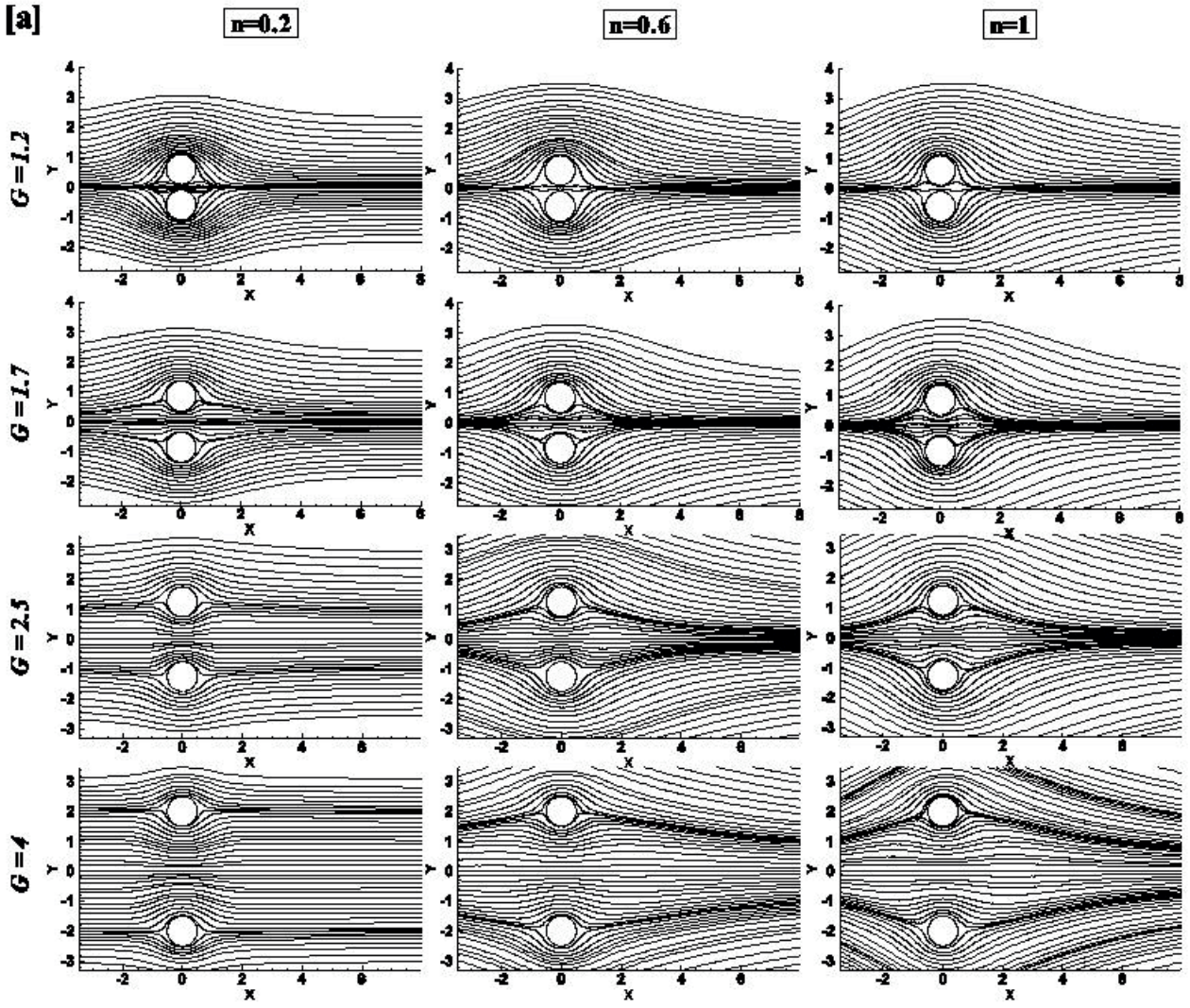

Figure 3. (a) Streamline contours for Re=0.1 at different G and n

bluff body irrespective of power-law index. When *Re* is increased to 10, vortices start forming at $n = 0$. Upon increasing the value of *Re* to 40, the wakes formed at $n = 0.6$ become larger in size compared to that formed at $Re = 10$. Simultaneous comparison of streamline profiles shown in Figure. 3 (c) and 3 (e) for $G = 1.2$ and $Re = 40$ shows that the size of the wake grows with an increase in the value of *n*, irrespective of the nature of the fluid (i.e., shear-thinning, Newtonian or shear-thickening). When *Re* is increased to 100, vortices become unstable at the rear region of the cylinder for $n = 0.2$ to 0.6. However, when *n* is increased to 1, vertices become stable and become symmetric about the mid plane with the formation of wakes.

It has already been mentioned that at $G = 1.2$ for low *Re* the streamline profiles obtained resemble the streamline profile obtained for a single bluff body irrespective of the power law index. When *G* is increased to little higher value, the streamline profiles follow a wider path, yet the flow field evoked by one cylinder is never independent of the other. At very high value of *G*, each cylinder behaves like an individual bluff body and creates a flow pattern without any influence of its neighboring cylinder. The shear thinning fluid with $n = 0.2$ can be an example to explain these phenomena. For $G = 1.2$ and at $Re = 0.1$, the flow profile almost resembles the flow profile evoked by a single bluff body. When the *G* is increased to 2.5 or 4, the streamline profile evoked by each cylinder resembles the streamline profile obtained for flow over a single cylinder. However, when $G = 1.7$, the streamline profile no longer resembles the streamline profile of a bluff body, neither does it look similar to that obtained at $G = 2.5$ or 4. The profile here is clearly influenced by the proximity of the cylinders. For the same fluid with $n = 0.2$, if the *Re* is increased from 0.1 to 40 and above, the streamline profile

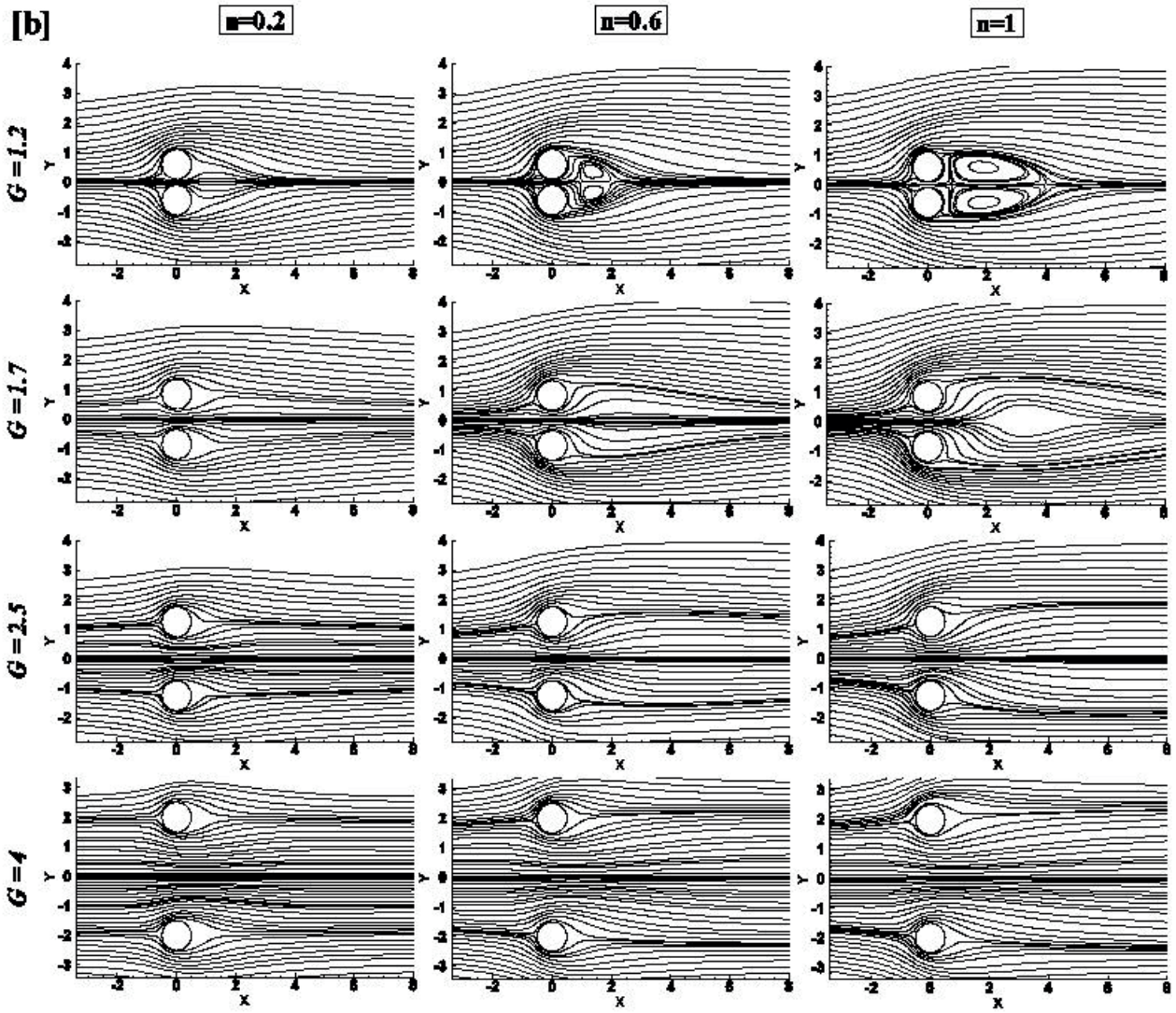

Figure 3. (b) Streamline contours for Re=10 at different G and n

obtained at G = 2.5 no longer looks like the streamline profiles of two individual cylinders. This implies that the streamline profiles are also influenced by *Re*. For instance, the velocity field decays rapidly in shear-thinning fluids, therefore very little interference is seen even up to *Re* = 10 and/or G = 1.2. On the other hand, the proximity of the two cylinders causes a boundary of the streamlines on the inner side of the cylinders, whereas that on the other side is seen to be influenced very little by the close proximity of the two cylinders. The fluid in the throat region experiences acceleration during the course of its passage through the nip region. The effect progressively diminishes with the increasing value of G. However, this asymmetry in the flow field gives rise to lift forces (in the y-direction) exerted on each cylinder. This asymmetry is seen to be present at all values of the Reynolds number, thereby leading to the formation of unequal sized standing vortices once the Reynolds number exceeds a critical value.

Surface Pressure Profiles

Figures 4 (a) and (b) show representative surface pressure profiles for both the upper and lower cylinders for a range of combinations of *Re*, G and n. Pressure profiles are shown over the entire surface ($0^0 \leq \theta \leq 360^0$) for both the cylinders. The profiles for *Re* = 100 are time-averaged profiles and, as discussed earlier, at least 10 constant periodic cycles are considered for the study. At low Reynolds numbers, e.g., at Re = 0.1, the surface pressure at the front region of the upper cylinder progressively increases with increasing degree of shear-thinning (decreasing value of n) and the same effect is observed for the lower cylinder. The minimum value of the pressure coefficient occurs at the point of separation (θ = ~900 and ~2800) for Re = 40 and 100, which is evident in both the cylinders. This is due to the recirculation nature of the flow at the rear of the cylinder. For Re = 40, as the value of G increases, the effect of power-law index seems to be less for both the cylinders.

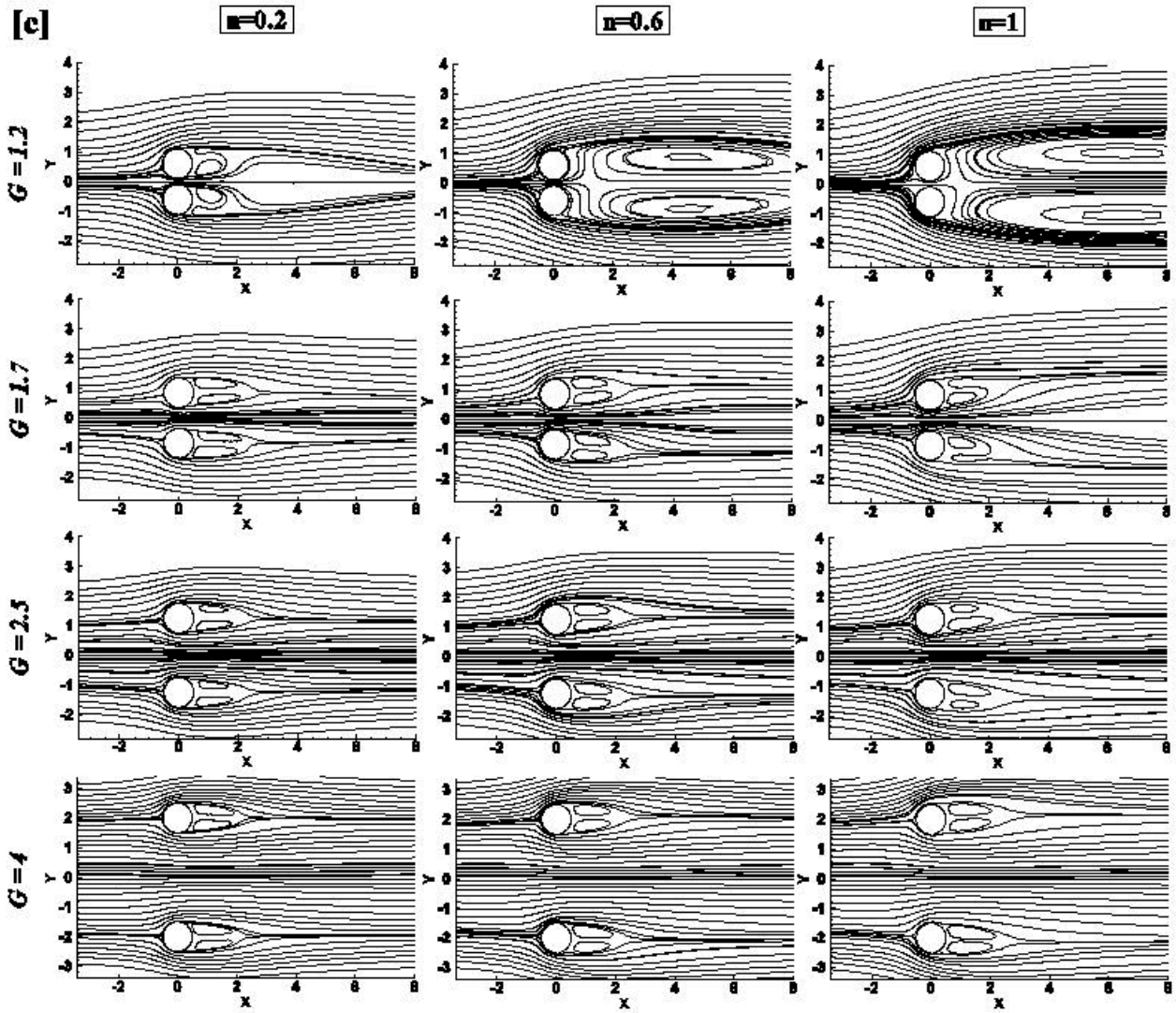

Figure 3. (c) Streamline contours for Re=10 at different G and n

At Re = 100, increasing G, the pressure decreases at the front region of both the cylinders. With increasing G, the effect of n decreases on the values of CP for Re = 40 and 100. The pressure is negative over most of the cases and this comes from different scaling of viscous and inertial forces on velocity and the power-law index.

Macroscopic Characteristics

The macroscopic characteristics of the flow are often presented by drag and lift coefficients. These characteristics in the steady state domain are discussed in the following sections.

Pressure Drag (C_{DP}) and Friction Drag (C_{DF}) Coefficients

Figure 5 (a) and (b) illustrate the influences of Reynolds number (*Re*), power-law index (*n*) and non-dimensional gap (*G*) on pressure drag (C_{DP}) and friction drag coefficients (C_{DF}). It is noted that the variation of *G* has an insignificant effect on C_{DP} and C_{DF}; on the other hand, the effect of Reynolds number is pronounced on these parameters. With an increase in Reynolds number, both C_{DP} and C_{DF} continuously decrease for all constant values of *n*. The effect of power-law index on C_{DP} and C_{DF} can also be noted from these figures (Figure 5 (a) and (b)). Figure 5 (a) indicates that, with an increase in the value of n, C_{DP} decreases continuously over the range *Re* = 0.1 - 40. The pressure drag coefficients (C_{DP}) for Newtonian fluid are always less than the shear-thinning one. On the other hand, with an increase in the value of *n*, C_{DF} decreases monotonously only in the range *Re* = 0.1 - 5. This shows that shear-thinning fluids exhibit stronger dependence on *Re* than Newtonian fluids. Therefore, a dramatic shift in trend is noticed in the high Reynolds number range, i.e., above *Re* > 5, where the value of C_{DF} increases with an increase in the value of *n*. It clearly shows that a Newtonian

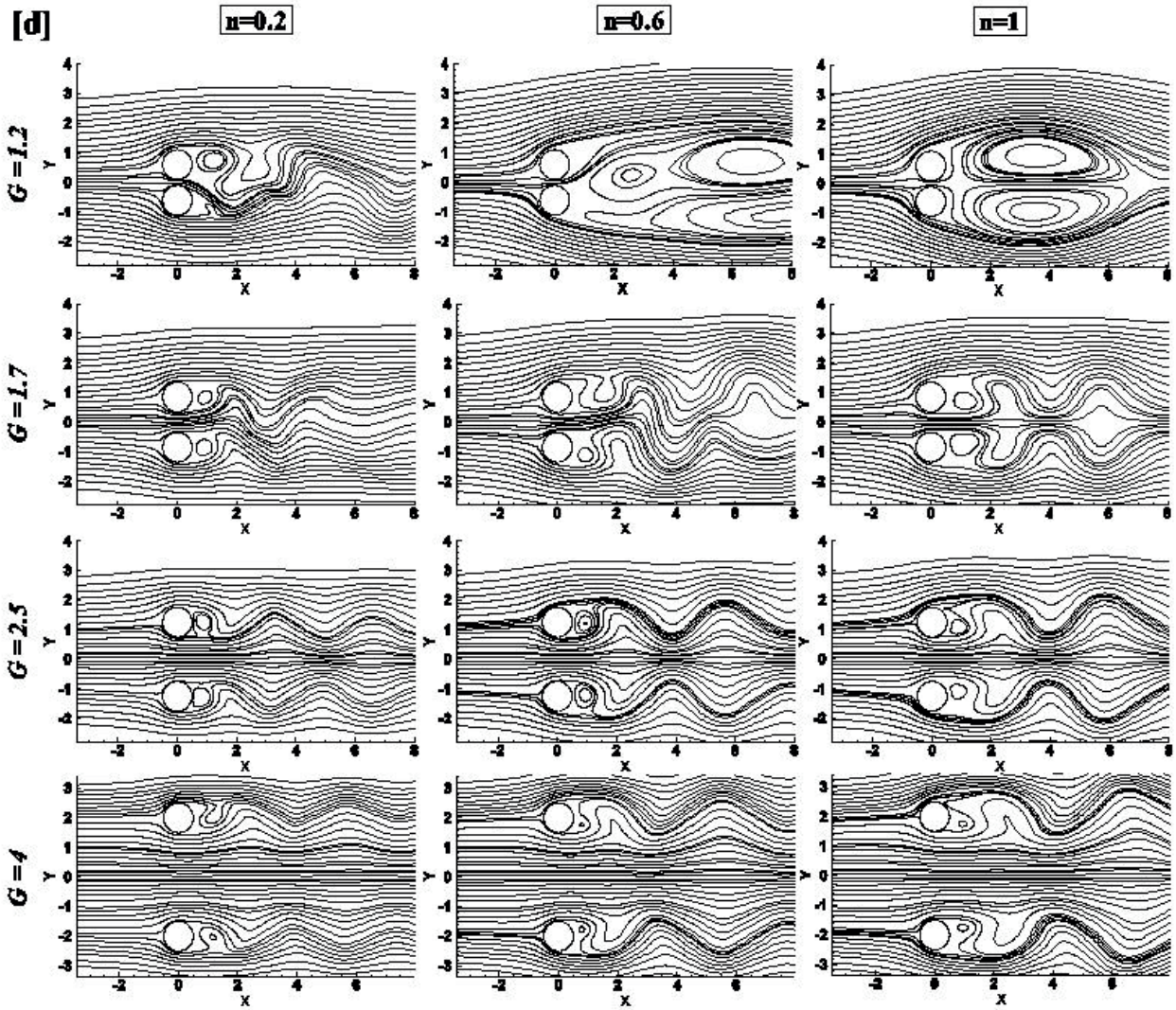

Figure 3. (d) Streamline contours for Re=100 at different G and n

fluid has higher friction drag coefficient than that of shear-thinning fluids. The similar trend in the flow pattern is noted for all values of *G*. To further analyze the behavior, the variations of (C_{DP}/ C_{DF}) at different values of *n*, *Re*, *G* are illustrated in Figure 6. From this figure, it can be seen that at high Reynolds number range the pressure drag (C_{DP}) is always higher than the friction drag (C_{DF}) for both Newtonian as well as power law fluids at the same value of *Re* and *G*.

Total Drag (C_D) Coefficients

The dependence of the total drag coefficients, C_D (= C_{DP} + C_{DF}), on the Reynolds number (*Re*) and the power-law index (*n*) for different gap ratios (*G*) is shown in Figure 7 (a). The value of total drag coefficient is approximately the same for both the cylinders. Therefore, a single figure (Figure 7) is used to represent the effect of drag coefficient. It is seen that, for constant *n* and *G*, an increase in *Re* decreases C_D.C_D becomes minimum at higher Re (*Re* = 40) for all the fluids over the entire range of G. The plot of C_D vs *Re* (Figure 7 (a)) has a striking similarity with the plot of C_{DP} vs *Re* (Figure 5 (a)). This similarity in the trend is attributed to the dominance of pressure drag coefficient over its counterpart friction drag coefficient over the entire studied range of *Re*, *n* and *G*. With an increase in *n* from 0.2 to 1, the C_D continuously decreases for all the conditions except in the range *Re* = 15-40 with G = 1.7- 4.

The variation in total drag coefficient (C_D) with gap ratio (*G*) for shear-thinning and non-Newtonian fluids at fixed values of *Re* is depicted in Figure 7 (b). From this figure it is clearly observed that in the low *Re* range the value of C_D is almost independent of *G* for both Newtonian and shear-thinning fluids. However, at high *Re*, especially at *Re* ≥ 10, C_D is found to be significantly influenced by *G*. At *Re* = 10, with an increase in *G,* the value of C_D increased constantly up to certain value where the growth of the C_D value ceased

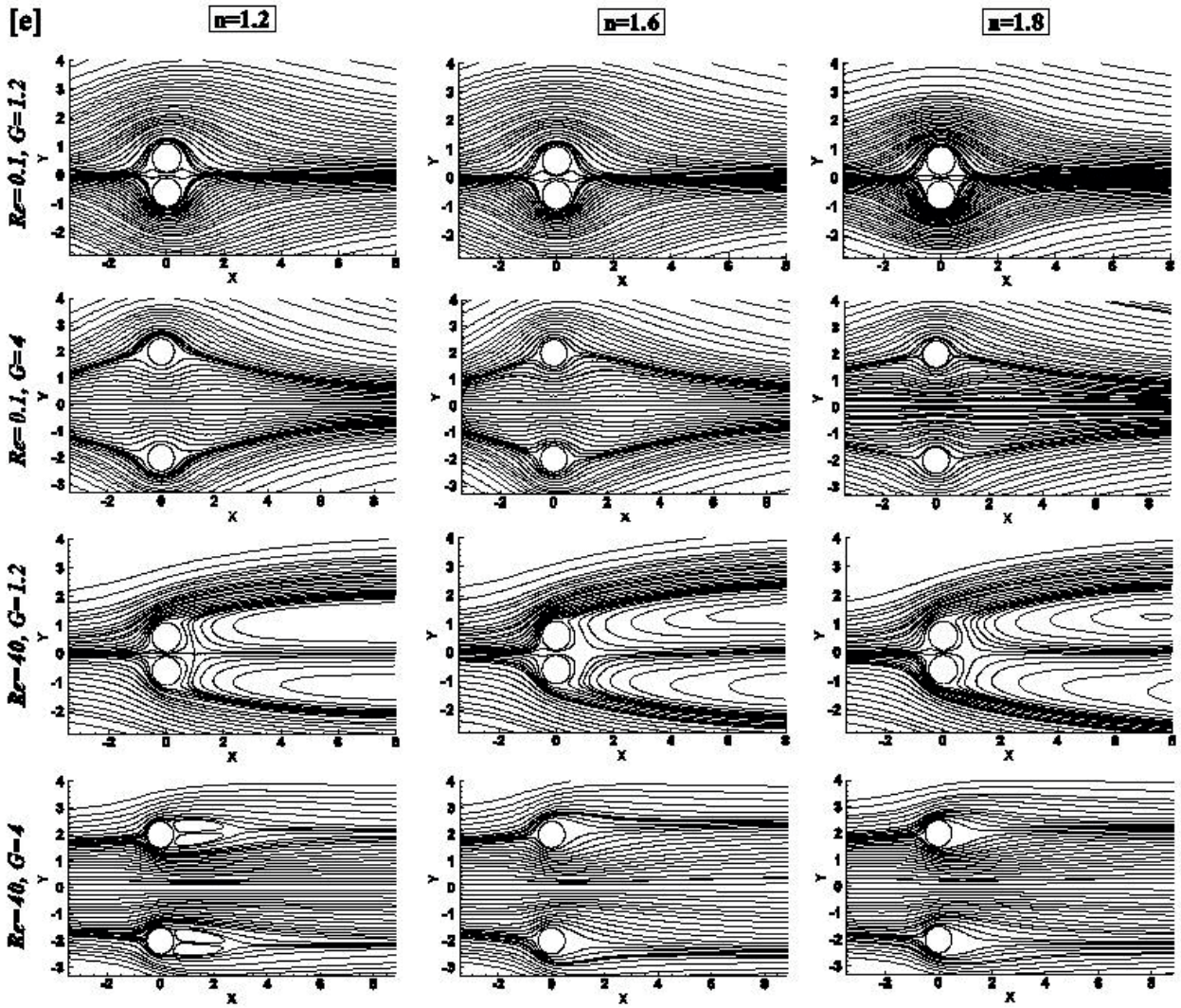

Figure 3. (e) Streamline contours for Re = 0.1, 40 at G = 1.2, 4 and n = 1.2, 1.6 and 1.8

(hereafter, this point is referred to as the critical value of G (G_c)). A further increase in the value of G beyond this critical value (G_c) does not influence the value of C_D. From the plots given for Re = 10 in Figure 7 (b), it can be noted that G_c depends on n. The value of the G_c for the power-law fluid with the smallest value of n is lower than that of the other fluids. On the other hand, at Re = 40, with an increase in G beyond G_c, the value of C_D decreases for both Newtonian and shear-thinning fluids. It needs to be noted here that G_c was never achieved for the power law fluid with n = 0.2 and the value of C_D continuously decreased with an increase in G. The rate at which the values of C_D decrease depends on n. The lower the power-law index, the higher the rate at which the value of C_D decreases with

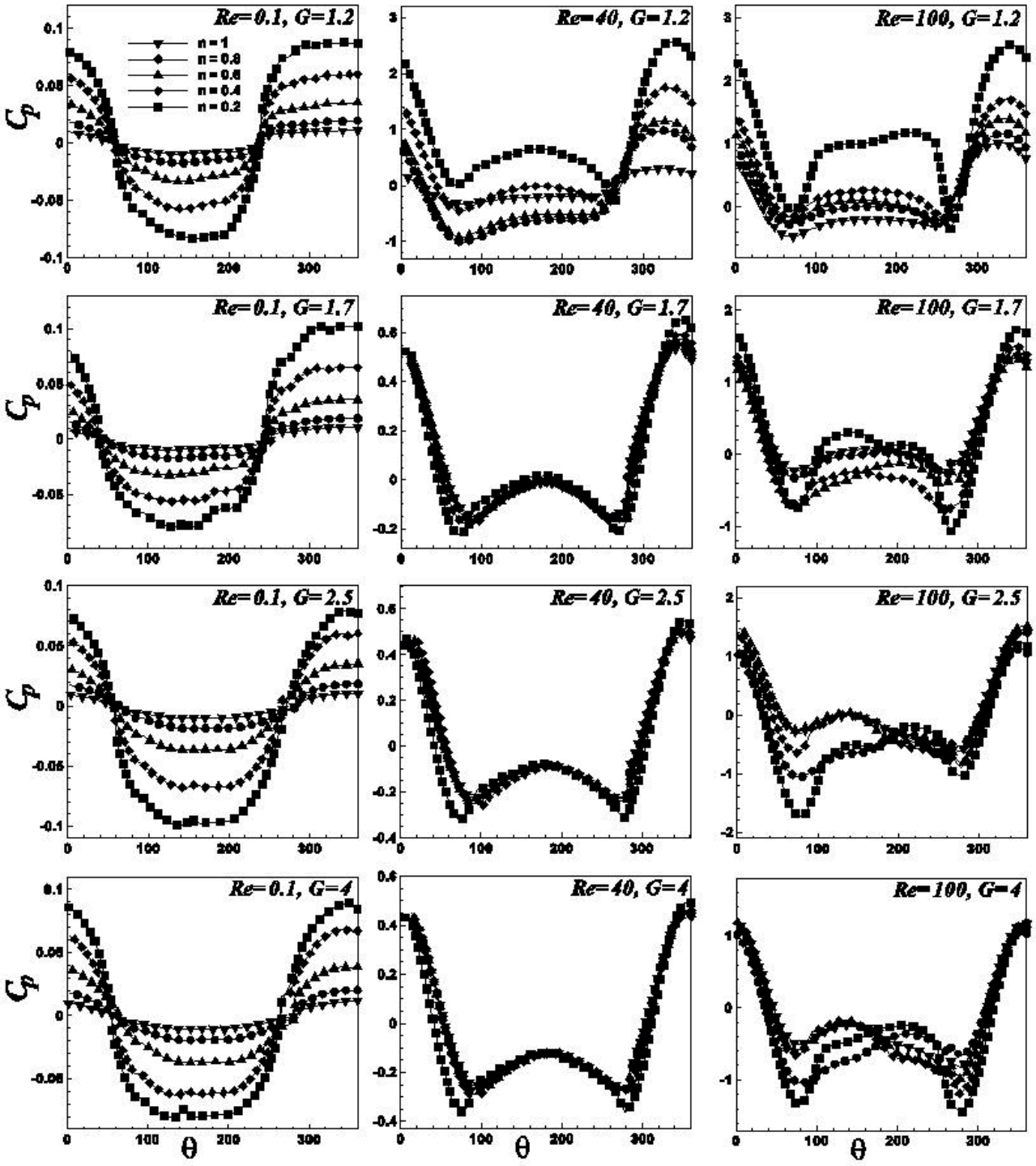

Figure 4 (a). Representative pressure profiles on the surface of the upper cylinder

increasing G. A comparison of the plots shown in Figure 7 (b) also indicates that at low Re, the C_D of shear-thinning fluid is higher than that of the Newtonian fluids. The value of C_D further decreases when shear-thickening fluid is used instead of Newtonian fluid (Figure 8). However, as the value of Re (especially above Re =10) increases the C_D of shear-thinning fluid decreases and becomes less than that of a Newtonian fluid. In this regime, the value of C_D remains highest for shear thickening fluid, which can be seen in Figure 8. This behavior is expected for shear-thinning fluid because with increased shearing/agitation in the flow, the resistance offered by the fluid reduces depending on the power-law index. The higher the power-law index, the higher is the resistance offered by the fluid in a similar environment.

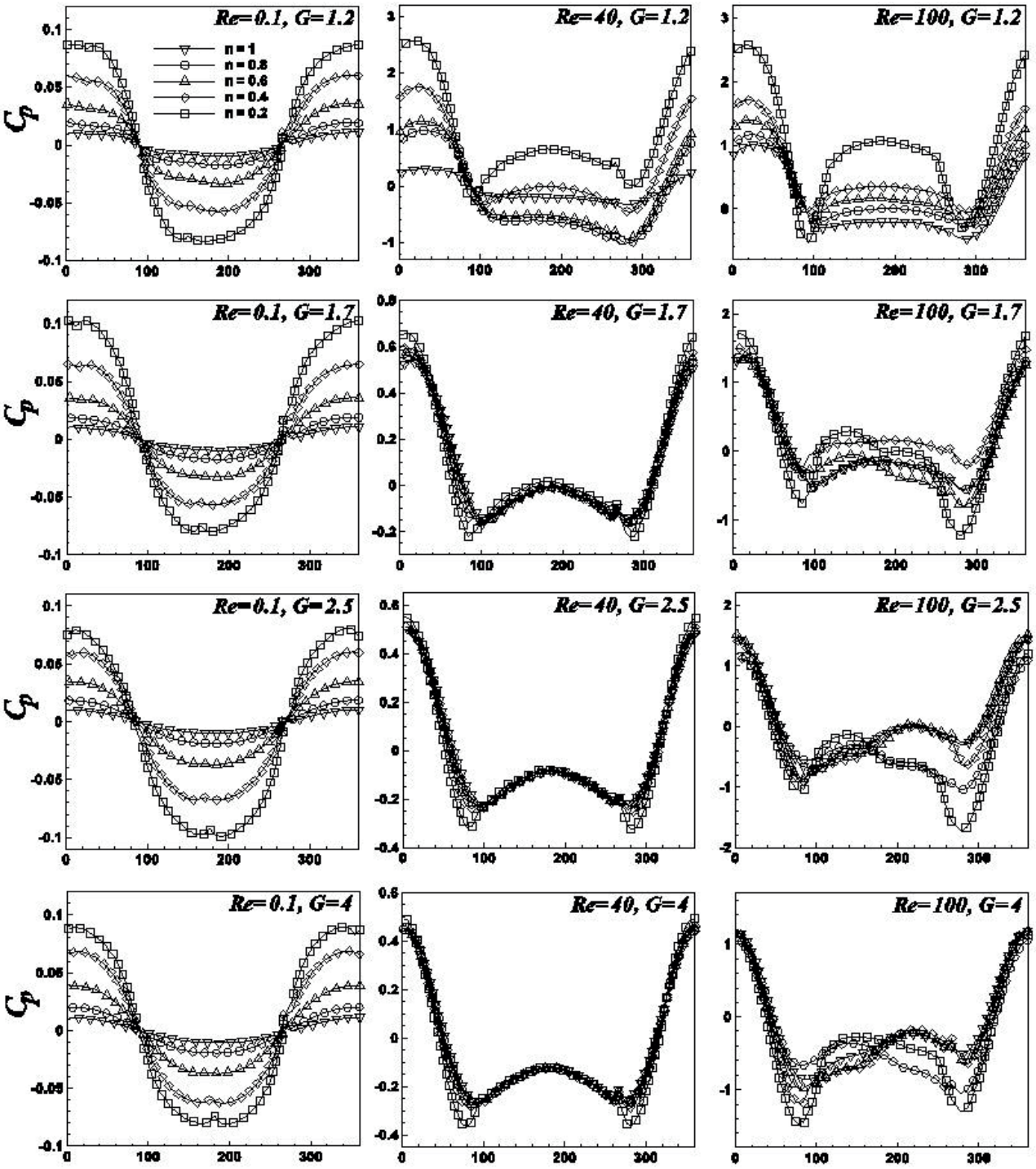

Figure 4 (b). Representative pressure profiles on the surface of the lower cylinder

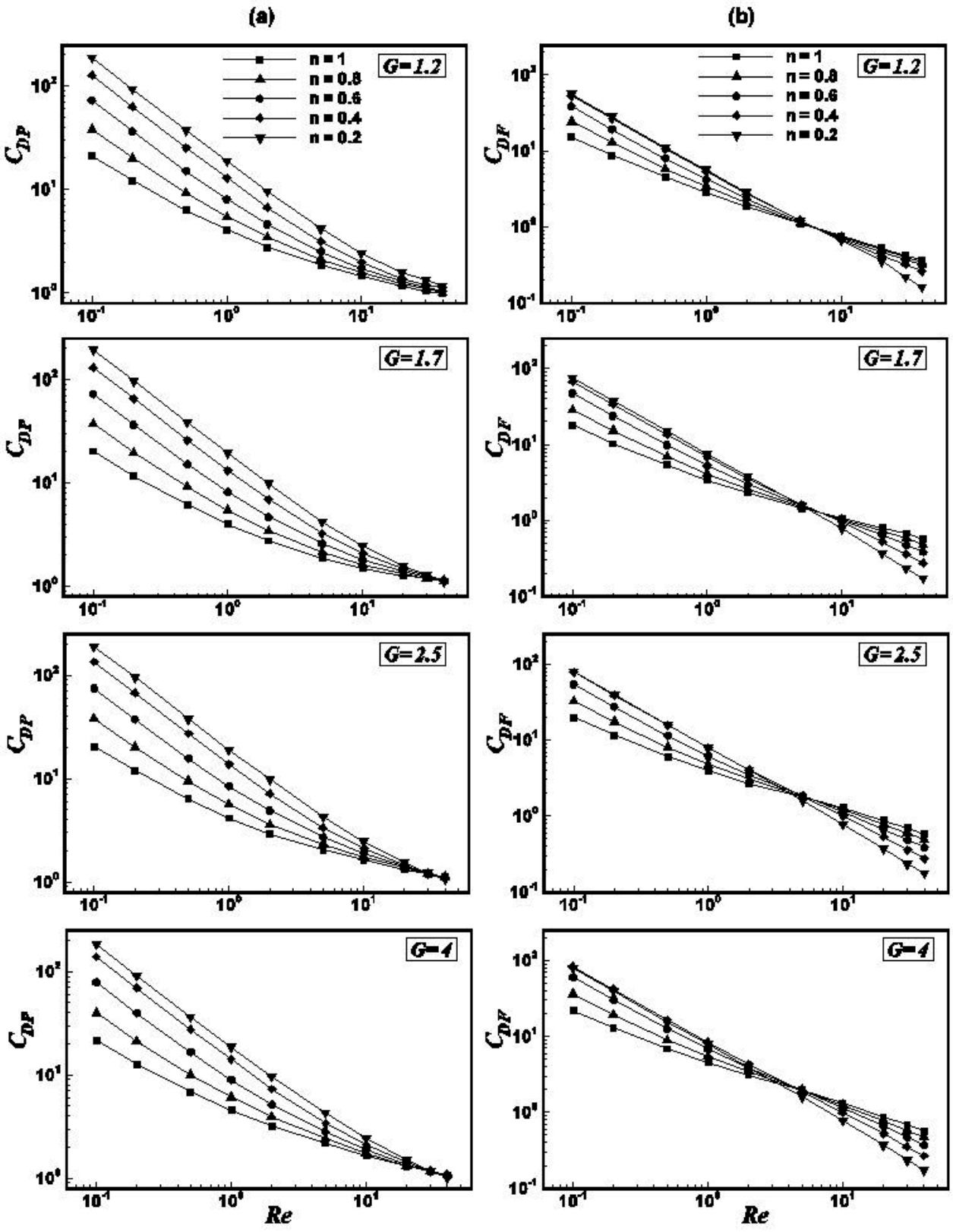

Figure 5. Variation of (a) pressure drag coefficient (C_{DP}) and (b) friction drag coefficient (C_{DF}) with Reynolds number (Re)

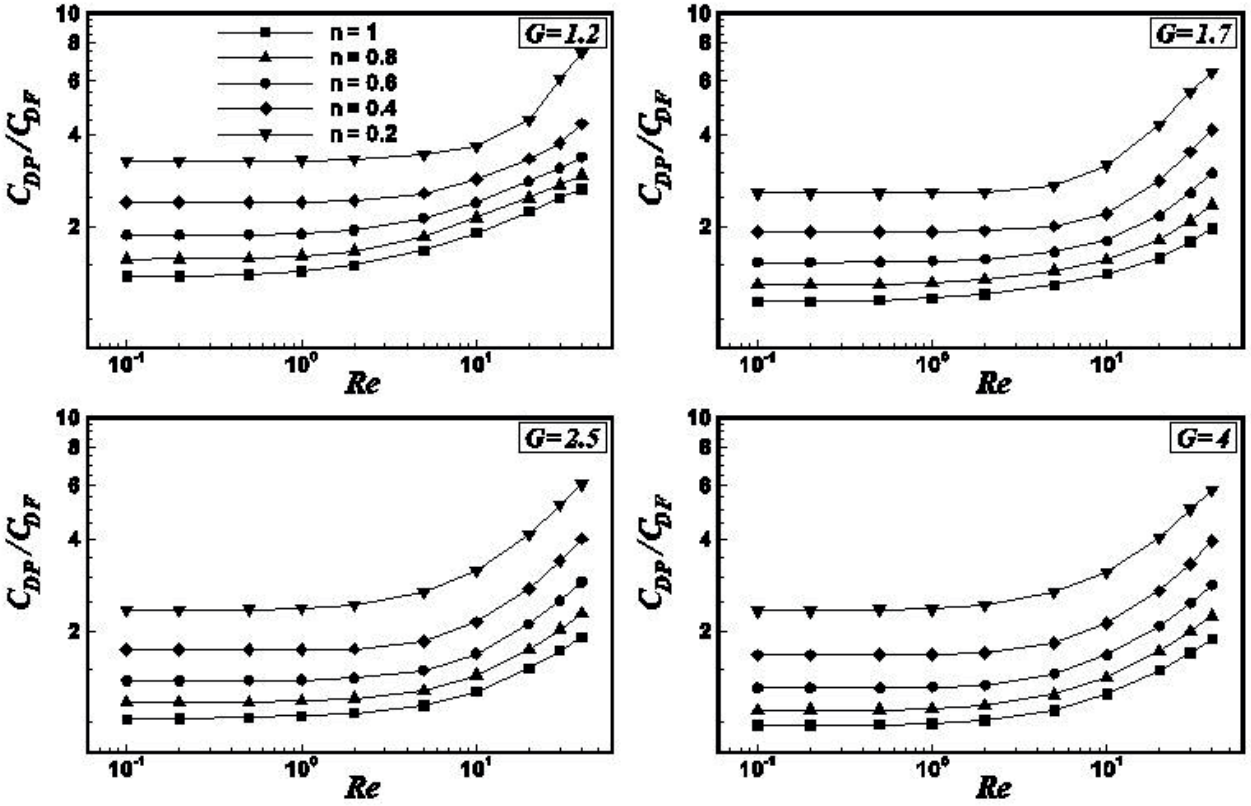

Figure 6. Variation of total lift coefficient (C_{DP}/C_{DF}) with Reynolds number (Re)

Since at very high gap ratio (G = 4) each cylinder almost behaves like an individual bluff body and creates a flow pattern without any influence of its neighboring cylinder, the comparison between C_D values obtained for twin cylinders with that obtained for an isolated cylinder is inevitable. Therefore, C_D values of the upper cylinder of the present case have been compared against the C_D values of an isolated cylinder (Panda and Chhabra, 2010) at some selected *Re* and *n* for gap ratio 4 (see Table 8). From the table it can be seen that there exists a difference in values of C_D for same values of *Re* and *n*. This difference in C_D values signifies the presence of some influence of the neighboring cylinder on the hydrodynamics, even though the streamline profile evoked by each cylinder resembles the streamline profile obtained for flow over a single cylinder.

Total Lift (C_L) Coefficients

Figure 9 shows the variation of the total lift coefficient with Reynolds number (*Re*) at different gap ratios (G) for each fluid. From the analysis of the results it is observed that the lift coefficients are the same for both the cylinders except the values are negative for the upper cylinder and positive for lower cylinders. Therefore, the values shown in Figure 9 can be used to represent the lift conditions of any of the cylinders, with the appropriate sign convention. For the easy analysis of the lift coefficient, the entire range of Reynolds number can be divided into three ranges; low *Re* range, medium *Re* range and high *Re* range.

***Low Re Range (0.1 ≤ Re ≤ 2)*:** In this range, for each fluid the value of C_L remains almost constant for a given G; an increase in *Re* value does not affect the value of the lift coefficient. On the other hand, the lift coefficient for Newtonian fluid monotonously decreases with an increase in *Re*, For shear thinning fluids, at low gap ratio the lift offered to the lower cylinder by the fluid with n = 0.2 is comparatively higher than that offered by other fluids. It can be noted from Figure 10 that with an increase in the value of n, C_L is found to decrease and achieve a minimum value at n = 0.6. With further increase in power law index to 1 and beyond, the value of C_L increases. With an increase in gap ratio the value of lift coefficient of this fluid (n = 0.2) continuously reduces. At G = 4, the C_L of this fluid with n = 0.2 attains a negative value. This signifies that at low gap ratio the fluid with power-law index n = 0.2 gives a positive lift and at high gap ratio it gives a negative lift to the cylinders which means the fluid tries to close the gap between the cylinders. On the other hand, at G = 4, the C_L value for all other fluids remains positive and continuously increases with an increase in n (see Figure 10).

***Medium Re Range (2 ≤ Re ≤ 20)*:** In this range, for a fixed gap ratio in the range G = 1.2 - 1.7, the value of a lift coefficient for all the fluids decreased with an increase in

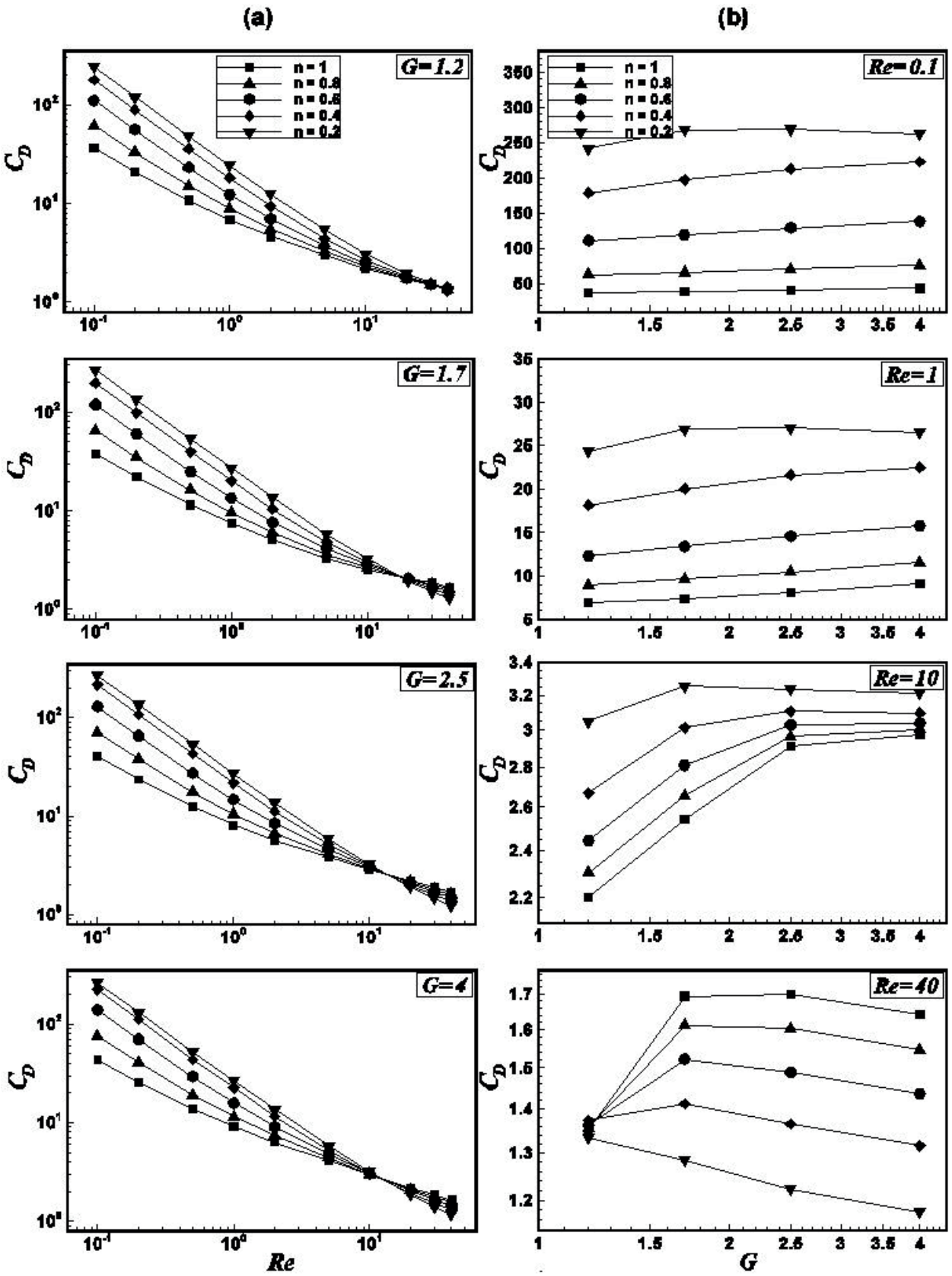

Figure 7. Variation of total drag coefficient (C_D) with (a) Reynolds number (Re) and (b) gap ratio (G)

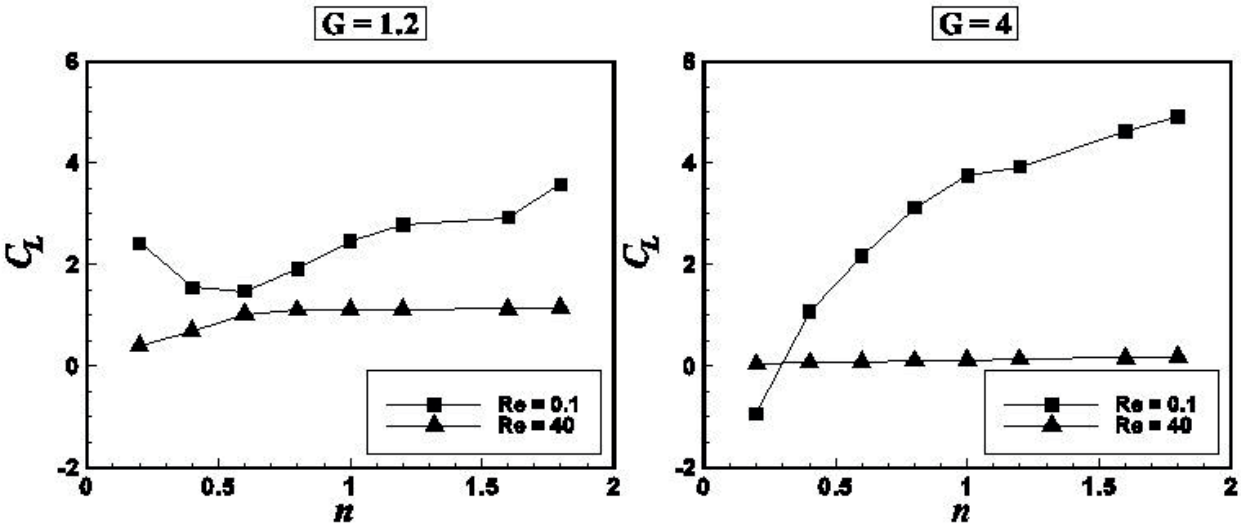

Figure 8. Variation of total drag coefficient (C_D) with power-law index for Reynolds number 0.1 and 40

Since at very high gap ratio (G = 4) each cylinder almost behaves like an individual bluff body and creates a flow pattern without any influence of its neighboring cylinder, the comparison between C_D values obtained for twin cylinders with that obtained for an isolated cylinder is inevitable. Therefore, C_D values of the upper cylinder of the present case have been compared against the C_D values of an isolated cylinder (Panda and Chhabra, 2010) at some selected *Re* and *n* for gap ratio 4 (see Table 8). From the table it can be seen that there exists a difference in values of C_D for same values of *Re* and *n*. This difference in C_D values signifies the presence of some influence of the neighboring cylinder on the hydrodynamics, even though the streamline profile evoked by each cylinder resembles the streamline profile obtained for flow over a single cylinder.

Total Lift (C_L) Coefficients

Figure 9 shows the variation of the total lift coefficient with Reynolds number (*Re*) at different gap ratios (*G*) for each fluid. From the analysis of the results it is observed that the lift coefficients are the same for both the cylinders except the values are negative for the upper cylinder and positive for lower cylinders. Therefore, the values shown in Figure 9 can be used to represent the lift conditions of any of the cylinders, with the appropriate sign convention. For the easy analysis of the lift coefficient, the entire range of Reynolds number can be divided into three ranges; low *Re* range, medium *Re* range and high *Re* range.

***Low Re Range (0.1 ≤ Re ≤ 2)*:** In this range, for each fluid the value of C_L remains almost constant for a given *G*; an increase in *Re* value does not affect the value of the lift coefficient. On the other hand, the lift coefficient for Newtonian fluid monotonously decreases with an increase in *Re*, For shear thinning fluids, at low gap ratio the lift offered to the lower cylinder by the fluid with n = 0.2 is comparatively higher than that offered by other fluids. It can be noted from Figure 10 that with an increase in the value of *n*, C_L is found to decrease and achieve a minimum value at n = 0.6. With further increase in power law index to 1 and beyond, the value of C_L increases. With an increase in gap ratio the value of lift coefficient of this fluid (n = 0.2) continuously reduces. At G = 4, the C_L of this fluid with n = 0.2 attains a negative value. This signifies that at low gap ratio the fluid with power-law index n = 0.2 gives a positive lift and at high gap ratio it gives a negative lift to the cylinders which means the fluid tries to close the gap between the cylinders. On the other hand, at G = 4, the C_L value for all other fluids remains positive and continuously increases with an increase in *n* (see Figure 10).

***Medium Re Range (2 ≤ Re ≤ 20)*:** In this range, for a fixed gap ratio in the range G = 1.2 - 1.7, the value of a lift coefficient for all the fluids decreased with an increase in Reynolds number. Similar trend is also noticed at G = 4 for all the fluids except the one with n = 0.2. In this range, the lift coefficient for the fluid with power-law index n = 0.2 increased and became positive. The rate at which the lift coefficient decreased or increased with *Re* depends on the power-law index.

***High Re Range (20 ≤ Re ≤ 40)*:** At low gap ratio, particularly at G = 1.2, the variation of C_L with *Re* shows similar characteristics as in the medium *Re* range. C_L increases with an increase in the value of *n* from 0.2 - 0.6. A further increase in the value of n does not affect the value of C_L. On the other hand as the value of *G* is increased, the lift coefficient again becomes independent of Re for each fluid. Also, the value of C_L also remains unaffected by the nature of the fluid (see Figure 10). For G = 4, at Re = 40, C_L becomes zero for all values of *n*, which is in complete

Table 8. Comparison of drag coefficient values between a single cylinder and the present case for Re = 0.1, 1 and 40 (G = 4)

C_D Single Cylinder (Panda and Chhabra, 2010)			C_D Upper Cylinder (Present work at G = 4)		
Re	***n* = 0.2**	***n* = 1**	***Re***	***n* = 0.2**	***n* = 1**
0.1	270.318	61.127	0.1	262.567	43.254
1	27.063	10.566	1	26.526	9.086
40	1.136	1.513	40	1.176	1.64

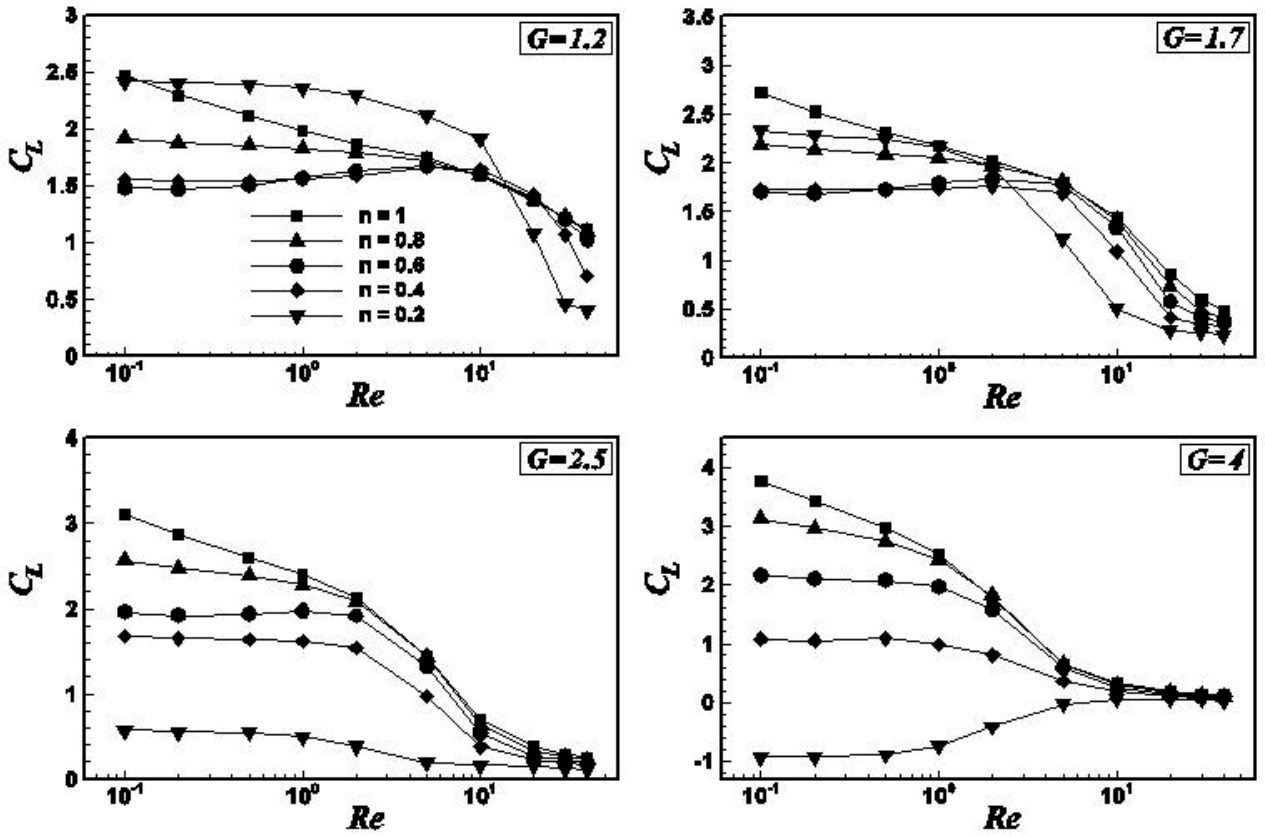

Figure 9. Variation of total lift coefficient (C_L) with Reynolds number (Re)

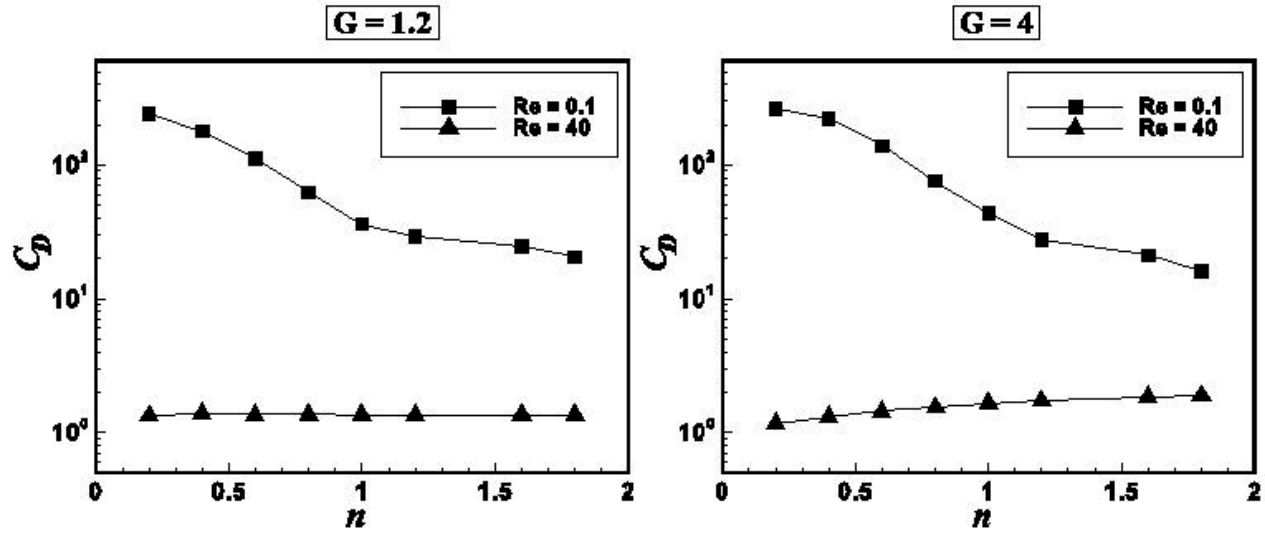

Figure 10. Variation of total lift coefficient (C_L) with power-law index for different Reynolds number 0.1 and 40

Reynolds number. Similar trend is also noticed at $G = 4$ for all the fluids except the one with $n = 0.2$. In this range, the lift coefficient for the fluid with power-law index $n = 0.2$ increased and became positive. The rate at which the lift coefficient decreased or increased with *Re* depends on the power-law index.

***High Re Range (20 ≤ Re ≤ 40)*:** At low gap ratio, particularly at $G = 1.2$, the variation of C_L with *Re* shows similar characteristics as in the medium *Re* range. C_L increases with an increase in the value of *n* from 0.2 - 0.6. A further increase in the value of n does not affect the value of C_L. On the other hand as the value of *G* is increased, the lift coefficient again becomes independent of Re for each fluid. Also, the value of C_L also remains unaffected by the nature of the fluid (see Figure 10). For $G = 4$, at $Re = 40$, C_L becomes zero for all values of *n*, which is in complete agreement with the values reported for a non-rotating isolated cylinder (Panda, 2010).

CONCLUDING REMARKS

The momentum characteristics of an unconfined laminar flow of shear-thinning fluids over a pair of cylinders in a side-by-side arrangement have been studied numerically over wide ranges of conditions as: $0.1 \leq Re \leq 100$, $0.2 \leq n \leq 1.8$ by varying gap ratios ($G = 1.2$, 1.7, 2, 2.5 and 4). The results reported here include the effect of Reynolds number (*Re*) and gap ratio (*G*) on the flow patterns, friction, pressure and total drag coefficients, lift coefficient and surface pressure coefficients for Newtonian and shear-thinning fluid flow. Reynolds number, power-law index and gap ratio significantly affect the streamline as well as the surface pressure coefficient of both the cylinders. From the analysis of results, it is also noted that at low *Re*, the total drag coefficient (C_D) of shear-thinning fluid is higher than that of the Newtonian and shear-thickening fluids. However, as the value of *Re* (especially above *Re* =10) increases, the C_D of shear-thinning fluid reduces and becomes less than that of Newtonian fluid. This behavior is attributed to the characteristic of shear-thinning fluid by virtue of which it offers less resistance to flow compared to a Newtonian fluid with increased agitation above a critical value of *Re*. The variation of lift coefficient (C_L) with *Re* divides the entire steady flow range into three different sub-ranges. In the low and high *Re* range, the lift coefficient remains almost independent of *Re*; in the medium Reynolds number range it shows a strong dependency on *Re*. Power law index (*n*) has a strong influence on the lift coefficient in both the low and medium *Re* range, whereas the effect of *n* becomes significantly weak on C_L in the high *Re* regime. On the basis of this study, for a specific fluid, the flow and gap ratio can be optimized to ensure the safety and stability of the components in industrial operations.

ACKNOWLEDGEMENTS

The author is sincerely grateful to Prof. R. P. Chhabra, Department of Chemical Engineering, Indian Institute of Technology, Kanpur for his guidance and support. The author also cordially acknowledges the valuable inputs and suggestions received from Dr. Dipti Samantaray, Indira Gandhi Centre for Atomic Research, Kalpakkam, India.

NOMENCLATURE

C_D	Drag coefficient, dimensionless
C_L	Lift coefficient, dimensionless
C_{DP}	Pressure component of drag coefficient, dimensionless
C_{DF}	Frictional component of drag coefficient, dimensionless
C_{LP}	Pressure component of lift coefficient, dimensionless
C_{LF}	Frictional component of lift coefficient, dimensionless
C_P	Pressure coefficient, dimensionless
D	Diameter of the cylinder (*m*)
f	Vortex shedding frequency (*Hz*)
F_D	Drag force per unit length of the cylinder (*N/m*)
C_{DP}	Pressure drag force per unit length of the cylinder (*N/m*)
F_{DF}	Friction drag force per unit length of the cylinder (*N/m*)
F_L	Lift force per unit length of the cylinder (*N/m*)
G	Gap ratio (= g/D), dimensionless
G_c	Critical gap ratio, dimensionless
g	Center-to-center distance between two cylinders (*m*)
H	Height (and width) of the square domain (*m*)
I_2	Second invariant of the rate of strain tensor (s^{-2})
L	Length of the cylinder (*m*)
m	Power-law consistency index ($Pa.s^n$)
n	Power-law flow behaviour index, dimensionless
n_s	Unit normal vector to the cylinder surface, dimensionless
N_i	Number of points on the surface of the cylinder
P	Pressure, dimensionless
R	Radius of the cylinder (*m*)
Re	Reynolds number, dimensionless
t	time, dimensionless
U_x	- Component of velocity, dimensionless
U_y	- Component of velocity, dimensionless
U_0	Uniform velocity of the fluid at inlet (*m/s*)
x, y	Cartesian co-ordinates, dimensionless

Greek letters

ρ	Density of the fluid (kg/m^3)

τ Shear stress (*Pa*)
τ_{ij} Shear stress (*Pa*)
μ Viscosity of the fluid (*Pa.s*)
ε_{ij} Component of the rate of strain tensor (s^{-1})
θ Angular position measured from the front stagnation point (*degree*)

Subscripts and superscripts
i, j *x*- and *y*- co-ordinates
∞ Free stream condition

REFERENCES

Astarita. G., Objective and generally applicable criteria for flow classification. J. Non-Newt. Fluid Mech., 6, 69-76 (1979).

Bearman, P. W., and Wadcock, A. J., The interaction between a pair of circular cylinders normal to a stream. J. Fluid Mech., 61, 499-511 (1973).

Bharti, R. P., Chhabra R. P., and Eswaran, V., Effect of blockage on heat transfer from a cylinder to power law liquids, Chem. Eng. Sci., 62, 4729-4741 (2007).

Bharti, R. P., Chhabra, R. P., and Eswaran, V., Steady flow of power-law fluids across a circular cylinder. Can. J. Chem. Eng., 84, 406-421 (2006).

Bharti, R. P., Chhabra, R. P., and Eswaran, V., Steady forced convection heat transfer from a heated circular cylinder to power-law fluids. Int. J. Heat Mass Transfer, 50, 977-990 (2007).

Bharti, R. P., Chhabra, R. P., and Eswaran, V., Two-dimensional steady Poiseuille flow of power-law fluids across a circular cylinder in a plane confined channel: Wall effects and drag coefficients. Ind. Eng. Chem. Res., 46, 3820-3840 (2007).

Bird, R. B., Armstrong, R. C., and Hassager, O., Dynamics of polymeric liquids. Volume 1; New York: Wiley (1987).

Bird, R. B., Stewart, W. E., and Lightfoot, E. N., Transport phenomena, 2nd edition, New York: John Wiley & Sons, Inc. (2002).

Bouaziz, M., Kessentini, S., and Turki, S., Numerical predictions of flow and heat transfer of power-law fluids in a plane channel with a built-in heated square cylinder. Int. J. Heat Mass Trans., 53, 5420-5429 (2010).

Chaitanya, N. S. K, and Dhiman, A. K., Non-Newtonian power-law flow and heat transfer across a pair of side-by-side circular cylinders. Int. J. Heat Mass Transfer, 55, 5941-5958 (2012).

Chhabra, R. P., Richardson J. F., Non-Newtonian flow in process industries: Fundamentals and Engineering Applications; Butterworth-Heinemann: Oxford (1999).

Chhabra, R. P., Soares, A. A., and Ferreira, J. M., Steady non-Newtonian flow past a circular cylinder: A numerical study. Acta Mech., 172, 1-16 (2004).

Coelho, P. M., and Pinho, F. T., Vortex shedding in cylinder flow of shear-thinning fluids II, Flow characteristics. J. Non-Newt. Fluid Mech., 110, 177-193 (2003).

D'Alessio, S. J. D., and Pascal, J. P., Steady flow of a power-law fluid past a cylinder. Acta Mech., 117, 87-100 (1996).

Ding, H., Shu, C., Yeo., K. S., and Xu., D., Numerical simulations of flows around two circular cylinder by mesh-free least square-based finite difference methods. Int. J. Num. Meth. Fluids, 53, 305-332 (2007).

Ghia, U., Ghia, K. N., and Shin, C.T., High-Re solutions for incompressible flow using the Navier-Stokes equations and a multigrid method, J. Comp. Phys., 48, 387-411 (1982).

Huang, Z., Olson, J. A., Kerekes, R. J., and Green, S. I., Numerical simulation of the flow around rows of cylinders. Comp. and Fluids, 35, 485-491 (2006).

Juncu, G., A numerical study of momentum and forced convection heat transfer around two tandem circular cylinders at low Reynolds numbers. Part I: Momentum transfer. Int. J. Heat Mass Transfer, 50, 3788-3798 (2007).

Juncu, G., A numerical study of momentum and forced convection heat transfer around two tandem circular cylinders at low Reynolds numbers. Part II: Forced convection heat transfer. Int. J. Heat Mass Transfer, 50, 3799-3808 (2007).

Kang, S., Characteristics of flow over two circular cylinders in a side-by-side arrangement at low Reynolds numbers, Phys. Fluids, 15, 2486-2498 (2003).

Khan, W. A., Culham, J. R., and Yovanovich, M. M., Fluid flow and heat transfer in power-law fluids across circular cylinders – Analytical study. J. Heat Transfer, 128, 870-878 (2006).

Liang, C., Papadakis, G., and Luo, X., Effect of tube spacing on the vortex shedding characteristics of laminar flow past an inline tube array: A numerical study. Comp. and Fluids, 38, 950-964 (2009).

Meneghini, J. R., Saltara, F., Siqueira, C. L. R, and Ferrari Jr., J. A., Numerical simulation of flow interference between two circular cylinders in tandem and side-by-side arrangements. J. Fluids Structures, 15, 327-350 (2001).

Morgan, V. T., The overall convective heat transfer from smooth cylinders. Adv. Heat Transfer, 11, 199-264 (1975).

Neofytou, P., A 3rd order upwind finite volume method for generalized Newtonian fluid flows, Adv. Eng. Soft., 36, 664-680 (2005).

Panda, S. K., and Chhabra, R. P., Laminar flow of power-law fluids past a rotating cylinder. J. Non-Newt. Fluid Mech., 165, 1442-1461 (2010).

Panda, S. K., Flow and heat transfer from a single and twin cylinder in power-law fluids. Master's Thesis, Indian Institute of Technology Kanpur, India (2010).

Panda, S. K., and Chhabra, R. P., Laminar forced convection heat transfer from a rotating cylinder to power-law fluids. Num. Heat Transer. A: Applications, 59, 297-319 (2011).

Patil, R. C., Bharti, R. P., and Chhabra, R. P., Steady flow of power law fluids over a Pair of cylinders in tandem arrangement. Ind. Eng. Chem. Res., 47, 1660-1683 (2008).

Patnana, V. K., Bharti, R. P., and Chhabra, R. P., Two dimensional unsteady flow of power-law fluid over a cylinder, Chem. Eng. Sci., 64, 2978-2999 (2009).

Patnana, V. K., Bharti, R. P., and Chhabra, R. P., Two dimensional unsteady forced convection heat transfer in power-law fluids from a cylinder, Int. J. Heat Mass Transfer, 53, 4152-4167 (2010).

Roache, P. J., Perspective: A method for uniform reporting of grid refinement studies, J. Fluids Eng., 116, 405-413 (1994).

Ryu, S., Lee, S. -B., Lee, B. -H., and Park, J. -C., Estimation of hydrodynamic coefficients for flow around cylinders in side-by-side arrangement with variation in separation gap. Ocean Engg., 36, 672-680 (2009).

Sahu, A. K., Chhabra, R. P., and Eswaran, V., Two-dimensional unsteady laminar flow of a power-law fluid across a square cylinder. J. Non-Newt. Fluid Mech., 160, 157-167 (2009).

Shyam, R., Sasmal, C., and Chhabra, R. P., Natural convection heat transfer from two vertically aligned circular cylinders in power-law fluids. Int. J. Heat Mass Transfer, 64, 1127-1152 (2013).

Sivakumar, P., Bharti, R. P., and Chhabra, R. P., Effect of Power-Law Index on Critical Parameters for Power-Law Flow across an Unconfined Circular Cylinder. Chem. Eng. Sci., 61, 6035-6046 (2006).

Sivakumar, P., Bharti, R. P., and Chhabra, R. P., Steady flow of power-law fluids across an unconfined elliptical cylinder. Chem. Eng. Sci., 62, 1682-1702 (2007).

Soares, A. A., Anacleto, J., Caramelo, L., Ferreira, J. M., and Chhabra, R. P., Mixed convection from a circular cylinder to power-law fluids. Ind. Eng. Chem. Res., 48, 8219-8231 (2009).

Soares, A. A., Ferreira, J. M., and Chhabra, R. P., Flow and forced convection heat transfer in cross flow of non-Newtonian fluids over a circular cylinder. Ind. Eng. Chem. Res., 44, 5815-5827 (2005).

Soares, A. A., Ferreira, J. M., Caramelo, L., and Anacleto, J., Effect of temperature-dependent viscosity on forced convection heat transfer from a cylinder in cross-flow of power-law fluids. Int. J. Heat Mass Transfer, 53, 4728-4740 (2010).

Srinivas, A. T., Bharti, R. P., and Chhabra, R. P., Mixed convection from a cylinder in power-law fluids: Effect of aiding buoyancy. Ind. Eng. Chem. Res., 48, 9735-9754 (2009).

Steffe, J. F., Rheological methods in food process engineering, 2nd edition, East Lansing, MI: Freeman (1996).

Thompson, R. L., and Mendes, P. R. S., Persistence of straining and flow classification. Int. J. Eng. Sci., 43, 79-105 (2005).

Tsutsui, T., An experimental study on heat transfer around two side-by-side closely arranged circular cylinders. J. Heat Transfer, 132, 111704-1 to 111704-8 (2010).

Whitney, M. J., and Rodin, G. J., Force velocity relationships for rigid bodies translating through unbounded shear-thinning power-law fluids. Int. J. Non-Linear Mech., 34, 947-953 (2001).

Williamson, C. H. K., Evolution of a single wake behind a pair of bluff bodies. J. Fluids Structures, 159, 1-12 (1985).

Zdravkovich, M. M., Review of flow interference between two circular cylinders in various arrangements. ASME J. Fluids Eng., 199, 618-633 (1977).

Zdravkovich, M. M., The Effects of interference between circular cylinders in cross flow. J. Fluids and Structures, 1, 239-261 (1987).

Zdravkovich, M. M., Flow around circular cylinders. Volume 1: Fundamentals; New York: Oxford University Press (1997).

Zdravkovich, M. M., Flow around circular cylinders. Volume 2: Applications; New York: Oxford University Press (2003).

Zhang, H. J., and Zhou, Y., Effect of unequal cylinder spacing on vortex street behind three side-by-side cylinders. Phys. Fluids, 13, 3675-3686 (2001).